

Postfire Snow Albedo and Forest Structure Recovery Drive Decadal Watershed Scale Reductions in Snow-Water Storage and Snow Retention

Anton James Surunis¹ and Kelly Gleason¹

¹Portland State University

June 1, 2023

Abstract

Forest fires darken snow albedo and degrade forest structure altering snowpack energy balance, peak snow volume and snowmelt timing for up to 15 years following burn. To date, three-dimensional volumetric estimates of postfire effects on snow hydrology over the course of postfire recovery have not been quantified at the watershed scale. Here we present an improved parameterization of recovery of forest fire effects on snow hydrology. Using a spatially-distributed snow mass and energy balance model called SnowModel, we estimate volumetric shifts in snow-water storage and snowmelt timing across a chrono-sequence of eight burned forests occurring between 2000 and 2019. One to three years following fire, postfire effects reduced peak snow-water storage by 8.42% on average (sd = 9.38%) and advanced snow disappearance date by 34 days on average (sd = 7 days). Magnitudes of snow disappearance date advances tended to decline over recovery relative to the losses observed immediately following fire. Postfire reductions in peak snow-water equivalent (SWE) tended to decrease immediately following fire, and generally recovered over 15 years postfire, but then increased again 4 to 9 years later. Postfire reductions on peak SWE summed over the 15-year postfire recovery period were up to eighteen times greater than the losses incurred in the first winter following fire alone. Beyond 15 years following fire, postfire effects on snow persisted due to the postfire shift from forest to open meadow.

Hosted file

963597_0_art_file_11014109_rv2qyx.docx available at <https://authorea.com/users/621716/articles/645171-postfire-snow-albedo-and-forest-structure-recovery-drive-decadal-watershed-scale-reductions-in-snow-water-storage-and-snow-retention>

1 **Postfire Snow Albedo and Forest Structure Recovery Drive Decadal Watershed Scale**
2 **Reductions in Snow-Water Storage and Snow Retention**

3 **A. Surunis¹ and K.E. Gleason²**

4 ¹ Department of Environmental Science and Management, Portland State University, Portland,
5 OR 97201; asurunis@pdx.edu.

6 ² Department of Environmental Science and Management, Portland State University, Portland,
7 OR 97201; k.gleason@pdx.edu.

8 Corresponding author: Anton Surunis (a.surunis@pdx.edu)

9 **Key Points:**

- 10 • Forest fire effects on snow hydrology parameterizations enabled basin-scale estimates of
11 postfire shifts in snow water storage and melt.
- 12 • Darkened snowpack and forest degradation decreased peak snow water storage by 4.5%
13 and snow retention by >8 days for 15 years postfire.
- 14 • Downstream snow-water resource availability is reduced in burned forested montane
15 watersheds across the western US for decades after fire.

16 **Keywords:** forest fire; snow water equivalent; snowmelt; snowmodel; modeling; forest structure;
17 western US; snow; snow albedo decay; snow albedo recovery

18 **Abstract**

19 Forest fires darken snow albedo and degrade forest structure altering snowpack energy balance,
20 peak snow volume and snowmelt timing for up to 15 years following burn. To date, three-
21 dimensional volumetric estimates of postfire effects on snow hydrology over the course of
22 postfire recovery have not been quantified at the watershed scale. Here we present an improved
23 parameterization of recovery of forest fire effects on snow hydrology. Using a spatially-
24 distributed snow mass and energy balance model called SnowModel, we estimate volumetric
25 shifts in snow-water storage and snowmelt timing across a chrono-sequence of eight burned
26 forests occurring between 2000 and 2019. One to three years following fire, postfire effects
27 reduced peak snow-water storage by 8.42% on average (sd = 9.38%) and advanced snow
28 disappearance date by 34 days on average (sd = 7 days). Magnitudes of snow disappearance date
29 advances tended to decline over recovery relative to the losses observed immediately following
30 fire. Postfire reductions in peak snow-water equivalent (SWE) tended to decrease immediately
31 following fire, and generally recovered over 15 years postfire, but then increased again 4 to 9
32 years later. Postfire reductions on peak SWE summed over the 15-year postfire recovery period
33 were up to eighteen times greater than the losses incurred in the first winter following fire alone.
34 Beyond 15 years following fire, postfire effects on snow persisted due to the postfire shift from
35 forest to open meadow.

36 **Plain Language Summary**

37 Forest fires in snowy regions burn away the forest canopy and drop burned woody debris onto
38 the snow below. The degradation of forest cover allows more sunlight to reach the snowpack and
39 the introduction of black carbon and burned woody debris onto snowpack darkens snow causing
40 it to absorb more sunlight energy. These two processes cause snow to melt earlier and disappear
41 sooner for up to 15 years following fire. We improved the ability of a snow-water model to
42 simulate immediate postfire effects on snow and the recovery of these effects over 15 years
43 following fire. We then quantified forest fire effects on snow volume and snow disappearance
44 date across eight forest fires occurring over a 20-year period in the Triple Divide region of
45 western Wyoming. We found that, in the winter immediately following fire, snow volume
46 decreased and snow disappeared 4-5 weeks sooner. When we summed postfire effects on snow
47 we found that postfire effects caused a 4.5% reduction in total snowpack over 15 years following
48 fire. Earlier snowmelt drives earlier peak streamflow, earlier drying of soils in spring, and leaves
49 surrounding forests drier for longer periods of time thereby increasing the likelihood of
50 summertime drought and future wildfire.

51 **1 Introduction**

52 The American West stores approximately 50-70% of its water in snowpack with flora, fauna, and
53 human populations relying on the slow and steady melting of this snow as a source of water in
54 the drier periods of late spring and summer (Li et al., 2017). Warming due to climate change has
55 reduced snow-water storage threatening annual water supply to downstream areas (Luce et al.,
56 2013; Mote et al., 2018; Wieder et al., 2022). Due to declining snowpacks, it is predicted that
57 spring surface water inputs will occur earlier and, without the buffering capacity provided by
58 snow, will occur less reliably and more episodically (Barnett et al., 2005; Hale et al., 2022;
59 Wieder et al., 2022).

60 Forest fires in the western United States occur predominately in the densely forested seasonal
61 snow zone where as much as 50% of western snow falls (Gleason et al., 2013). The frequency,

62 severity, and extent of forest fire in the West has been increasing due to rising air temperatures
63 and subsequent effects on seasonal snowpack and summertime soil moisture (Westerling, 2016).
64 Forest fire in the seasonal snow zone modifies forest structure and introduces black carbon onto
65 snow, altering the snowpack energy balance and snow ablation (Gleason et al., 2019). Canopy
66 removal by wildfire reduces shading, subjecting greater surface areas of snow to increased solar
67 shortwave radiative inputs and increasing wind-driven sublimation losses (Ueyama et al., 2014).
68 Canopy removal also reduces longwave radiative inputs from vegetation, but in continental
69 snowpack these reductions can often be counteracted by the additional inputs of solar radiative
70 forcing due to reduced shading and increased wind ablative losses (Lundquist et al., 2013;
71 Musselman et al., 2008; Varhola et al., 2010). In continental regions, where temperatures are
72 colder and longwave radiative inputs from vegetation are reduced, additional solar radiative
73 inputs from reductions in shading tend to outweigh the losses in longwave radiative inputs from
74 forest structure degradation and result in a net increase in shortwave radiative forcing on
75 snowpack (Lundquist et al., 2013; Musselman et al., 2008; Varhola et al., 2010). Forest fire
76 deposition of black carbon and burned woody debris onto snowpack darkens snow albedo,
77 enhancing shortwave radiative forcing on snowpack from the more open postfire forest structure,
78 the rate of snow metamorphism and, subsequently, the rate of snow albedo decay following fresh
79 snowfall (Gleason et al., 2013, 2019; Gleason & Nolin, 2016). Together, forest fires impact snow
80 hydrology through direct and indirect reductions in snow albedo and forest structure degradation,
81 resulting in increased postfire radiative forcing on snow, altered snowpack energy balance,
82 decreased peak snow water equivalent (SWE), and earlier snow disappearance date (SDD) for at
83 least 10-15 years following fire (Gersh et al., 2022; Gleason et al., 2019; Smoot & Gleason,
84 2021; Stevens, 2017).

85 The difficulty in quantifying postfire impacts on snow over large temporal and spatial scales
86 using in-situ measurements make remotely sensed measurements a valuable tool in monitoring
87 snow properties in remote regions over broad spatial scales. Gersh et al. (2022) utilized remote
88 sensing derived estimates of landscape snow albedo from the National Aeronautics and Space
89 Administration's (NASA) Moderate Resolution Imaging Spectroradiometer (MODIS)
90 instrument's landscape snow albedo product (MOD10A1) to analyze trends in the long-term
91 recovery of snow albedo following forest fire in the Triple Divide Region of Wyoming (Gersh et
92 al., 2022). Results showed that landscape snow albedo steadily recovered back to an unburned
93 open meadow state over the course of 15 years, with much of the recovery occurring in the first
94 10 years following the initial burn (Gersh et al., 2022). However, assessment of fine-scale snow
95 albedo trends using MODIS data are limited by coarse resolutions and the presence of
96 obstructions such as clouds or canopy. MODIS-MOD10A1 data are provided at a coarse spatial
97 resolution of 500m and are not able to measure snow albedo values through clouds or other
98 obstructions such as canopy cover (Armitage et al., 2013; Hall & Riggs, 2007; Riggs et al.,
99 2017). Measurements of snow albedo can be influenced by fine scale landcover variability
100 resulting in mixed pixels that do not accurately represent the albedo in a given grid cell (e.g.,
101 patchy snow cover can artificially reduce albedo measurements) (Campagnolo et al., 2016;
102 Cescatti et al., 2012) and variability in cloud cover can result in long periods where little to no
103 data can be retrieved from a particular study region (Armitage et al., 2013; Hall & Riggs, 2007;
104 Riggs et al., 2017). The limited spatial extent of in-situ measurements and coarse resolution of
105 remotely sensed measurements make process-based snow evolution models that incorporate such
106 data an important tool in quantifying the long-term effects of forest fire on snow at a watershed
107 scale.

108 To quantify the watershed-scale forest fire effects on snow-water storage and snowmelt, we used
109 a spatially-distributed snow evolution model called SnowModel. SnowModel is a process-based
110 model that uses first-order physics to simulate snow accumulation; blowing-snow redistribution
111 and sublimation; snow-density evolution; and snowpack melt over spatially varying topography
112 and landcover grids driven by temporally varying meteorological forcing fields (Liston et al.,
113 2007; Liston & Elder, 2006a, 2006b). SnowModel was used in this study because of its basis in
114 first-order physics, ready customizability, and extensive validation in forested, montane seasonal
115 snowpack similar to our study region (Hiemstra et al., 2006; Liston et al., 2007, 2008; Liston &
116 Elder, 2006a, 2006b; Sexstone et al., 2018). SnowModel utilizes four sub-models in a hierarchal
117 modeling structure: MicroMet, EnBal, SnowPack-ML, and SnowTran-3D. MicroMet spatially
118 interpolates meteorological forcing data from met stations observations and/or modeled
119 reanalysis met outputs of air temperature, precipitation, wind speed, wind direction, air pressure,
120 and relative humidity (Liston & Elder, 2006a). Using a spatially weighted Barne's interpolation
121 method, MicroMet produces a meteorological forcing field for every cell in the simulation for
122 every time step (Liston & Elder, 2006b). MicroMet also estimates incoming shortwave and
123 longwave radiation inputs in each cell using solar calculations based on the latitude of the study
124 region and parametrizations of cloudiness (Liston & Elder, 2006a). EnBal utilizes the outputs of
125 MicroMet and physics-based mass energy balance equations to calculate the snow mass and
126 energy balance of the snowpack within every cell at every time step of the simulation and,
127 critical to our application, is where modeling of forest-snow interactions are handled (Liston &
128 Hall, 1995). SnowTran-3D is a three-dimensional model that incorporates the wind-flowing
129 forcing field from MicroMet and topographical and vegetation inputs to compute redistribution
130 of snow due to wind and loss of snow by saltation and wind-induced sublimation (Liston et al.,
131 2007). SnowPack-ML computes snow-density through temperature- and compaction-based
132 snow-density evolution (Liston & Elder, 2006b). SnowPack-ML can be run using a single layer
133 or up to 12 distinct layers and simulates cold content, permeability, and liquid water release from
134 the snowpack within each cell for every time step (Liston & Elder, 2006b).

135 To date, research has shown that forest fires in the seasonal snow zone alter snow-water storage
136 and snowmelt for at least 10-15 winters following ignition (Gleason et al., 2013, 2019; Smoot &
137 Gleason, 2021). However, these studies have focused on point based or broad scale estimations,
138 and no studies have quantified the watershed-scale postfire effects on snow hydrology at a fine
139 spatial resolution and over the decades-long postfire recovery period using a physically based
140 snow evolution model. Here, we modeled and quantified postfire impacts on snow-water storage
141 and snowmelt metrics, including peak SWE, total snow volume, and SDD, over a
142 chronosequence of eight forest fires occurring in the Triple Divide region of northwestern
143 Wyoming. by incorporating a postfire effect on snow albedo and forest structure and recovery
144 parameterization into SnowModel.

145 Our postfire effect on snow albedo decay and forest structure and recovery model utilized a
146 parameterization of postfire effects on snow albedo and snow albedo decay from Gleason and
147 Nolin (2016) and a postfire forest structure degradation and snow albedo recovery model
148 informed by long-term trends in MODIS-derived landscape snow albedo (LSA) from Gersh et al.
149 (2022). The parameterization of postfire effects on snow albedo and snow albedo decay was
150 drawn from a study by Gleason and Nolin (2016) which derived empirical snow albedo decay
151 functions from broadband snow albedo measurements taken in adjacent burned and unburned
152 forested sites in the Shadow Lake burn region (ignition date: 2011) in the Oregon Cascades up to
153 3 years following fire. The parameterizations from this study characterized snow albedo decay as

154 an exponential function of days since snowfall for both burned and unburned forested sites and
155 for both positive net energy balance periods (accumulation) and negative net energy balance
156 periods (ablation) respectively for a total of four snow albedo decay functions (Gleason & Nolin,
157 2016). The long-term (1-15 years postfire) snow albedo recovery trends were informed by Gersh
158 et al. (2022) which characterized postfire snow albedo recovery over years since fire in a chrono-
159 sequence of eight burns occurring in the Triple Divide region of Wyoming between 2000 and
160 2018, the same burns modeled in this study. The study by Gersh et al. (2022) utilized MODIS-
161 MOD10A1 estimates of landscape snow albedo (LSA) within the eight burn regions for up to 15
162 years following fire and determined, through Tukey analysis, that LSA values within the burn
163 regions shifted to LSA values similar to that of nearby open regions over the course of 15 years
164 following fire. The findings of these two studies provided the basis for our improved postfire
165 snow albedo decay and recovery parameterization.

166 By incorporating postfire effects on snow albedo and forest structure and the associated recovery
167 into a mechanistic model, we evaluated postfire effects on snow-water storage and snowmelt
168 immediately following fire and over the course of a 15-year recovery period both within each
169 forest fire perimeter and at the watershed scale. Understanding and quantifying how postfire
170 effects on snow albedo and forest structure affect snow hydrology over many years following
171 fire is vital as snowpacks continue to warm and forest fires increase in occurrence and extent
172 across the West. The modeling approach and findings discussed here will help to improve
173 understanding of the broad scale and lasting implications of forest fire effects on snow-water
174 storage and snowmelt timing in headwaters critical for spring and summertime water supply.

175 **2 Materials and Methods**

176 **2.1 Study Region**

177 We evaluated the recovery of postfire effects on snow albedo and forest structure, and the
178 associated effects on snow hydrology across a chronosequence of eight forest fires in the
179 seasonal snow zone of Western Wyoming which burned between 2000 and 2018. The study area
180 covers the Triple Divide region of three major river basins of the western US, including the
181 Colorado, Columbia, and Missouri Rivers, and was determined by calculating a minimum
182 bounding rectangle around the chronosequence of the forest fire perimeters. Forest fire
183 perimeters were defined using the Monitoring Trends in Burn Severity (MTBS) burn perimeters
184 data (Finco et al., 2012) plus a 2 km buffer determined within ArcGIS (Figure 1). The study
185 domain has an average elevation of 2503m (sd = 320m) with a minimum and maximum
186 elevation of 1727m and 3596m respectively (Danielson & Gesch, 2010). Between 2000 and
187 2020, the average cold season (December to March) air temperature was -7.7°C (sd = 5.5°C)
188 and the region received an average precipitation of 3.0 mm (sd = 4.94 mm) (NOAA, 2021; Saha
189 et al., 2011; *USDA-NRCS*, 2020; Western Regional Climate Center, 2021). The study region is
190 largely forested, consisting of 60% forested land and 40% unforested land (35% shrub,
191 grassland, and agricultural, 0.006% urban, and 4% bare rock) based on Copernicus Global

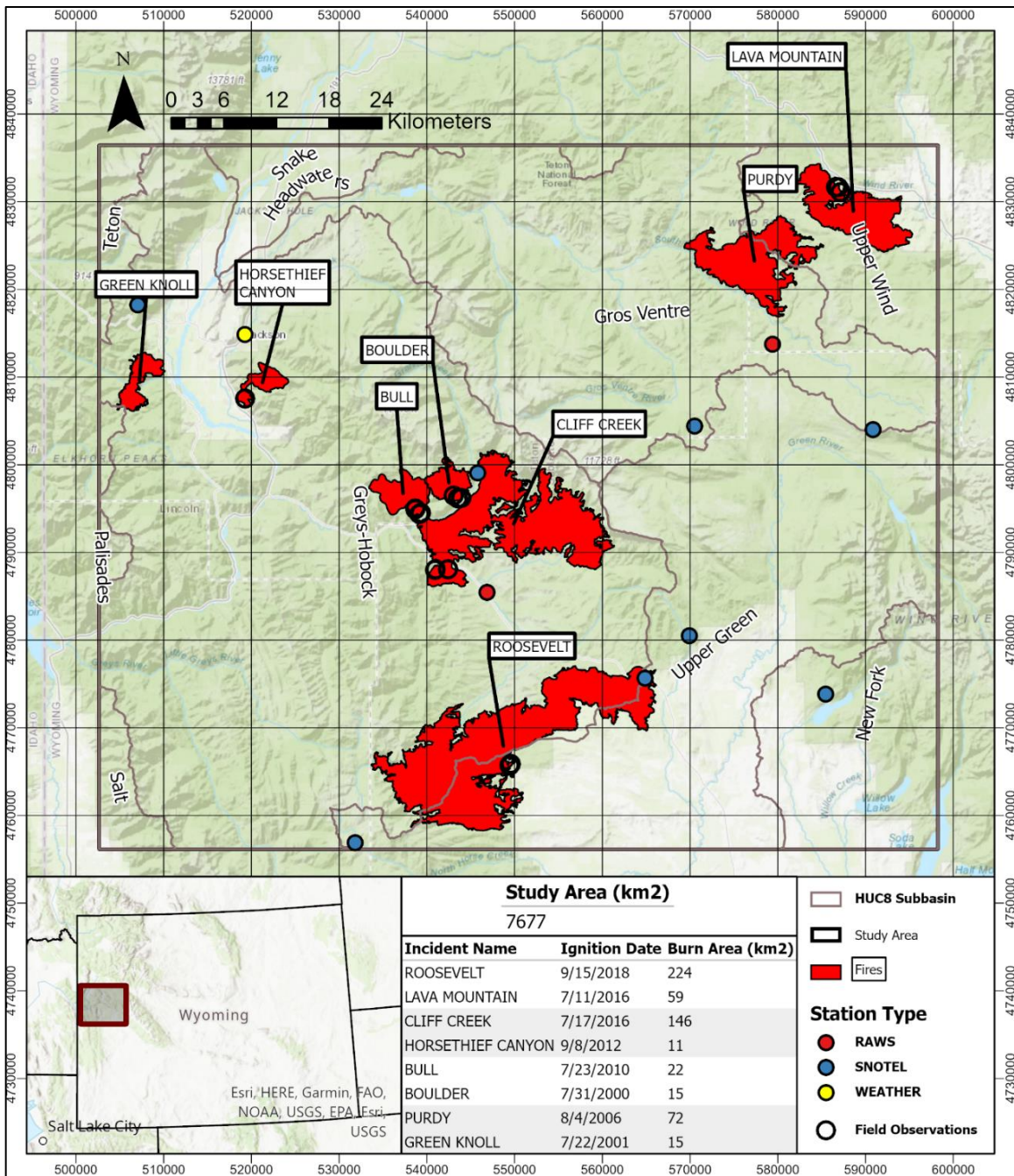


Figure 1: A map of the study region and modeling domain. The map includes Monitoring Trends in Burn Severity fire boundaries of the eight fires that occurred in the study region over the modeling time period along with their ignition date, incident type, and total burn area. The location and type of meteorological stations that the in-situ meteorological forcing data was drawn from are shown and the boundaries of the HUC-8 sub-basins and their names are also displayed.

192 Landcover data (Buchhorn et al., 2020). The forested land is pine-dominated, of which the most
 193 common species are Lodgepole Pine (*Pinus contorta*) and Whitebark Pine (*Pinus albicaulis*).

194 The study area includes the Triple Divide headwaters of three major river basins in the western
 195 US, widening the hydrological implications of forest fire effects on snow hydrology within this

196 area. Further, the study area has a history of frequent forest fire and has experienced a rapid
 197 increase in the extent, severity, duration, and occurrence of forest fire in the seasonal snow zone
 198 over the last decade. The combination of these two features along with the area receiving 60-
 199 80% of its annual precipitation as snow (Serreze et al., 1999) makes investigation of postfire
 200 effects on snow hydrology critical to preserving snow-water resources within this region and for
 201 understanding postfire effects on snow throughout the West.

202 2.2 SnowModel Input Data Retrieval

203 SnowModel requires three major inputs: meteorological forcing data, a topographic elevation
 204 raster, and a landcover classification raster. Meteorological forcing data was retrieved from both
 205 automated weather stations and modeled reanalysis data. In-situ meteorological forcing data
 206 from automated weather stations were retrieved from the United States Department of
 207 Agriculture (USDA) National Resources Conservation Service’s (NRCS) automated Snow
 208 Telemetry (SNOTEL) network (USDA-NRCS, 2020) via the National Weather and Climate
 209 Center (NWCC) data retrieval tool (<https://wcc.sc.egov.usda.gov/reportGenerator>). SNOTEL
 210 data were supplemented with additional in-situ weather data from the Western Regional Climate
 211 Center’s (WRCS) Remote Automated Weather Station (RAWS) network (Western Regional
 212 Climate Center, 2021), and the National Oceanic and Atmospheric Administration’s (NOAA)
 213 Climate Data Online (CDO) network (NOAA, 2021) to capture a wider range of weather
 214 variability over elevation (Table 1). Hourly measurements of air temperature, precipitation, wind
 215 speed, wind direction, and relative humidity were retrieved from each of these stations and daily
 216 average values of each metric were calculated for use in SnowModel. In addition, daily SWE
 217 values were retrieved from the nine SNOTEL stations for SWE assimilation and later calibration
 218 of SnowModel.

219 The in-situ meteorological data were supplemented with data from Climate Forecast System
 220 version 2 (CFSv2) modeled reanalysis meteorological data from the NOAA National Centers for
 221 Environmental Prediction (NCEP) (Saha et al., 2011). CFSv2 pixels were converted into
 222 “virtual” weather stations using R’s (R Core Team, 2021) “spatial” package (v7.3-12; Venables
 223 & Ripley, 2002), where the coordinates of each “station” was taken as the centroid of the pixel
 224 and elevation was taken as a product of geopotential height at surface. This process effectively

Table 1: List of meteorological stations used as the meteorological forcing data input or as validation data in SnowModel. Relevant metadata is provided including station type, data source, station ID number (* = validation station only), elevation in meters, easting and northing coordinates (CRS: NAD83 UTM12N), and date of the start of record.

Station Name	Type	Source	Station ID	Elevation (m)	Easting (m)	Northing (m)	Start of Record
Blind Bull Sum	SNOTEL	USDA-NRCS	353*	2637	531829	4756891	10/1/1978
East Rim Divide	SNOTEL	USDA-NRCS	460*	2417	564881	4775668	10/1/1984
Granite Creek	SNOTEL	USDA-NRCS	497*	2063	545799	4799058	10/1/1987
New Fork Lake	SNOTEL	USDA-NRCS	689*	2542	507065	4818219	10/1/1984
Gros Ventre Summit	SNOTEL	USDA-NRCS	506	2667	570509	4804425	4/1/1976
Gunsight Pass	SNOTEL	USDA-NRCS	555	2993	579829	4788969	9/1/1998
Kendall R.S.	SNOTEL	USDA-NRCS	597	2359	569894	4780482	10/1/1984
Loomis Park	SNOTEL	USDA-NRCS	661	2512	585471	4773860	10/1/1979
Phillips Bench	SNOTEL	USDA-NRCS	944	2499	590870	4803994	3/1/1976
Hoback Wyoming	RAWS	DRI-WRCS	481302	2050	546858	4785438	6/1/1996
Raspberry Wyoming	RAWS	DRI-WRCS	481307	2682	579399	4813724	6/1/1985
Jackson Airport	Weather	NOAA-CDO	USC00484910	1893	519283	4814846	1/1/1893

225 produced an ordered grid of weather stations across the study region. Daily values of
226 temperature, precipitation, wind speed, and wind direction were averaged from measurements
227 CFSv2 captures each day, and relative humidity was computed using daily averaged specific
228 humidity value, daily average temperature, and the Clausius-Clapeyron relation (Brown, 1951).

229 Digital elevation maps (DEMs) and landcover classifications were retrieved using Google Earth
230 Engine (Gorelick et al., 2017), a cloud-based and free-to-use GIS software. A DEM of the region
231 was retrieved from the Global Multi-resolution Terrain Elevation Dataset (GMTED) 2010
232 (Danielson & Gesch, 2010). GMTED is a product of NASA's Shuttle Radar Topography Mission
233 (SRTM), which generated a digital elevation model of elevation data at a resolution of 1 arc-
234 second. Landcover data was retrieved from the Copernicus Global Land Cover 2015-2019
235 dataset which classifies 23 different classes of landcover data at a 100m resolution (Buchhorn et
236 al., 2020). Landcover data was reclassified to match the land classes recognized by SnowModel.
237 Both raster layers were clipped to the study region, used at their native resolutions of 100m, and
238 converted to ASCII using R's (R Core Team, 2021) "spatial" package (v7.3-12; Venables &
239 Ripley, 2002).

240 2.3 SnowModel Calibration

241 SnowModel was calibrated by running the base model iteratively using different sets of
242 parameters for gap fraction, snow fraction calculations, number of snowpack layers and
243 snowpack layer width, and scalars applied to air temperature and precipitation forcing data.
244 Following each run, modeled SWE values were compared with the time-series of observed SWE
245 values obtained from the SNOTEL stations within the study region. For calibration purposes,
246 four of the nine SNOTEL stations were excluded from the meteorological inputs to use as a
247 validation-only set. Modeled values of SWE at the observation locations were extracted by
248 locating the cell containing each SNOTEL station and the associated observed SWE measured
249 by the SNOTEL station for that time step. Modeled SWE depth (SWED) was then compared to
250 the observed SNOTEL measurements using root-squared error, normalized squared error, R-
251 squared, and percent bias (Moriasi et al., 2007). Pixel values were extracted using the "spatial"
252 package (v7.3-12; Venables & Ripley, 2002) within R (R Core Team, 2021) and the
253 performance statistics were calculated using the "HydroGOF" package (v0.4-0; Mauricio
254 Zambrano-Bigiarini, 2020). Following 21 calibration runs, ideal parameters were found that met
255 the performance thresholds outlined by Moriasi et al (2007) (Table 2). The best calibration was
256 found using the default parameters of SnowModel, but with the modeled precipitation inputs
257 increased by 18.5%, an amount consistent with previous research from Yuan et al (2011) that
258 found that CFSv2 modeled reanalysis data can underestimate precipitation results by up to 20%.
259 After calibration, SnowModel overestimated SWE by 11.40% across all stations, a level of
260 overestimation acceptable given the performance thresholds determined by Moriasi et al (2007)
261 ($|PBIAS| < 15\%$) (Table 2).

262 2.4 Model Descriptions

263 To quantify spatially and temporally distributed forest fire effects on snow hydrology, we used
264 the improved postfire recovery of snow albedo and forest structure modeled over a
265 chronosequence of burned forests in the Triple Divide region of western Wyoming. We
266 developed three models to quantify how postfire effects on snow albedo, snow albedo decay, and

Table 2: Table showing the final performance statistics of SnowModel following pre-parameterization calibrations. The four statistics (described in the Preliminary Results section) are shown for each of the nine SNOTEL stations within the study region and the overall performance statistics are shown on the last row. The performance thresholds used for this study are also shown for each of the four statistics.

Station Name	Station ID	Elevation (m)	Eastings (m)	Northing (m)	Start of Record	RSR (<0.70)	NSE (>0.50)	R ² (>0.60)	PBIAS (x <15%)
Blind Bull Sum	353*	2637	531829	4756891	10/1/1978	0.34	0.89	0.90	5.10
East Rim Divide	460*	2417	564881	4775668	10/1/1984	1.03	-0.06	0.81	60.80
Granite Creek	497*	2063	545799	4799058	10/1/1987	0.29	0.91	0.93	-6.10
New Fork Lake	689*	2542	507065	4818219	10/1/1984	0.57	0.68	0.77	11.80
Gros Ventre Summit	506	2667	570509	4804425	4/1/1976	0.68	0.54	0.87	28.50
Gunsight Pass	555	2993	579829	4788969	9/1/1998	0.31	0.90	0.95	-14.60
Kendall R.S.	597	2359	569894	4780482	10/1/1984	0.28	0.92	0.92	2.20
Loomis Park	661	2512	585471	4773860	10/1/1979	0.34	0.89	0.93	10.20
Phillips Bench	944	2499	590870	4803994	3/1/1976	0.49	0.76	0.90	23.10
Overall						0.44	0.81	0.85	11.40

267 forest structure degradations alter snow volume and snowmelt timing over the decades-long
 268 postfire recovery period. These models included a base model, an improved postfire snow
 269 albedo recovery model, and a combined postfire snow albedo and forest structure recovery
 270 model.

271 2.4.1 Base model

272 The base model used the default, calibrated SnowModel parameters to compare against the
 273 results of the postfire forest structure and postfire snow albedo recovery models, but
 274 supplemented with the unburned forest snow albedo decay parameterizations from Gleason &
 275 Nolin (2016). The based model snow albedo decay parameterization applied time-varying
 276 exponential decay of snow albedo over days since snowfall differentially to unburned forests and
 277 open meadows during snow accumulation and snow melt periods. The base model included a
 278 snow albedo decay function but represented a simulation of the study region for 20 years with no
 279 postfire effects incorporated.

280 2.4.2 Postfire forest structure model

281 The postfire forest structure model consisted of the base model with the addition of time-varying
 282 postfire forest structure degradation parameterizations that simulated the degradation of forest
 283 structure over 15 years following fire towards that of an open meadow (Equation 3 below), but
 284 with no postfire effects on snow albedo or snow albedo decay included. The postfire forest
 285 structure model allowed for compartmentalization of postfire effects on snow hydrology due to
 286 forest structure changes versus postfire effects on snow hydrology due to postfire effects on
 287 snow albedo and snow albedo decay. The postfire forest structure model simulated only the
 288 postfire effects of forest structure degradation over 15 years without postfire effects on snow
 289 albedo.

290 2.4.3 Postfire snow albedo recovery model

291 The postfire snow albedo recovery model consisted of both an improved version of the time-
 292 decay of snow albedo parameterizations from Gleason & Nolin (2016) (Equations 1 and 2
 293 below) as well as the forest structure degradation parameterizations from the postfire forest
 294 structure model (Equation 3). In short, this model simulated the postfire effects on snow albedo,

295 snow albedo decay, and forest structure and recovered these parameters to that of an open
 296 meadow over the course of 15 years following fire.

297 2.4.4 Parameterizations of postfire recovery of snow albedo and forest structure

298 Five sets of snow albedo minima and maxima, snow albedo decay functions, and forest structure
 299 parameters were computed by calculating five equally spaced values between those of an
 300 immediate postburn forest and an unburned open meadow. Snow albedo minimum and
 301 maximum and snow albedo decay curves for both a burned forest and an unburned open meadow
 302 were drawn from Gleason & Nolin (2016), while forest structure was parameterized using
 303 SnowModel's snow-holding depth values for scattered conifer forests and open meadows as the
 304 immediate postfire state and post-recovery state, respectively. The snow-holding depth is used in
 305 SnowModel to calculate the snow holding capacity of vegetation within each grid cell. The snow
 306 depth of a cell must exceed this value before snow can reach the ground and become available
 307 for wind redistribution and be subjected to wind ablation effects and canopy-modified solar
 308 forcing. In order to represent the postfire snow albedo recovery, our parameterization includes
 309 five recovery stages each representing 3 years of recovery in five unique snow albedo recovery
 310 stages over the 15 year postfire recovery period (Figure 2). The 3-year recovery stages postfire
 311 snow albedo functions and forest structure parameters were applied to each burned forest by
 312 assigning custom burned forest classes using spatially distributed annual landcover rasters.

313 The improved postfire snow albedo and forest structure recovery parameterization solves for
 314 daily mean snow albedo using a time-varying exponential decay coefficient, where the minimum
 315 and maximum snow albedo values, and the degree of decay are modified to recover over fifteen
 316 years by the five recovery periods following forest fire. The parameterization resets snow albedo
 317 values following a fresh snowfall event (>5cm), and then exponentially decays over days
 318 following snowfall using recovery stage specific coefficients. Maximum snow albedo ($\alpha_{snow,max}$)
 319 represents the snow albedo of fresh snowfall in a burned forest as calculated by Gleason & Nolin
 320 (2016). Maximum snow albedo postfire recovery rate ($\Delta\alpha_{snow,max}$) is defined as the difference
 321 between $\alpha_{snow,max}$ and the snow albedo of fresh snowfall in an unburned open meadow divided by
 322 five (the number of three-year recovery periods in 15 years of postfire recovery). The fresh
 323 snowfall recovery rate is scaled by the number of 3-year recovery periods since forest fire (p)
 324 and added to $\alpha_{snow,max}$ to produce the snow albedo of fresh snowfall in a recovering forest fire
 325 (Equation 1).

$$326 \quad \alpha_{snow} = \alpha_{snow,max} + (p * \Delta\alpha_{snow,max}) \quad (1)$$

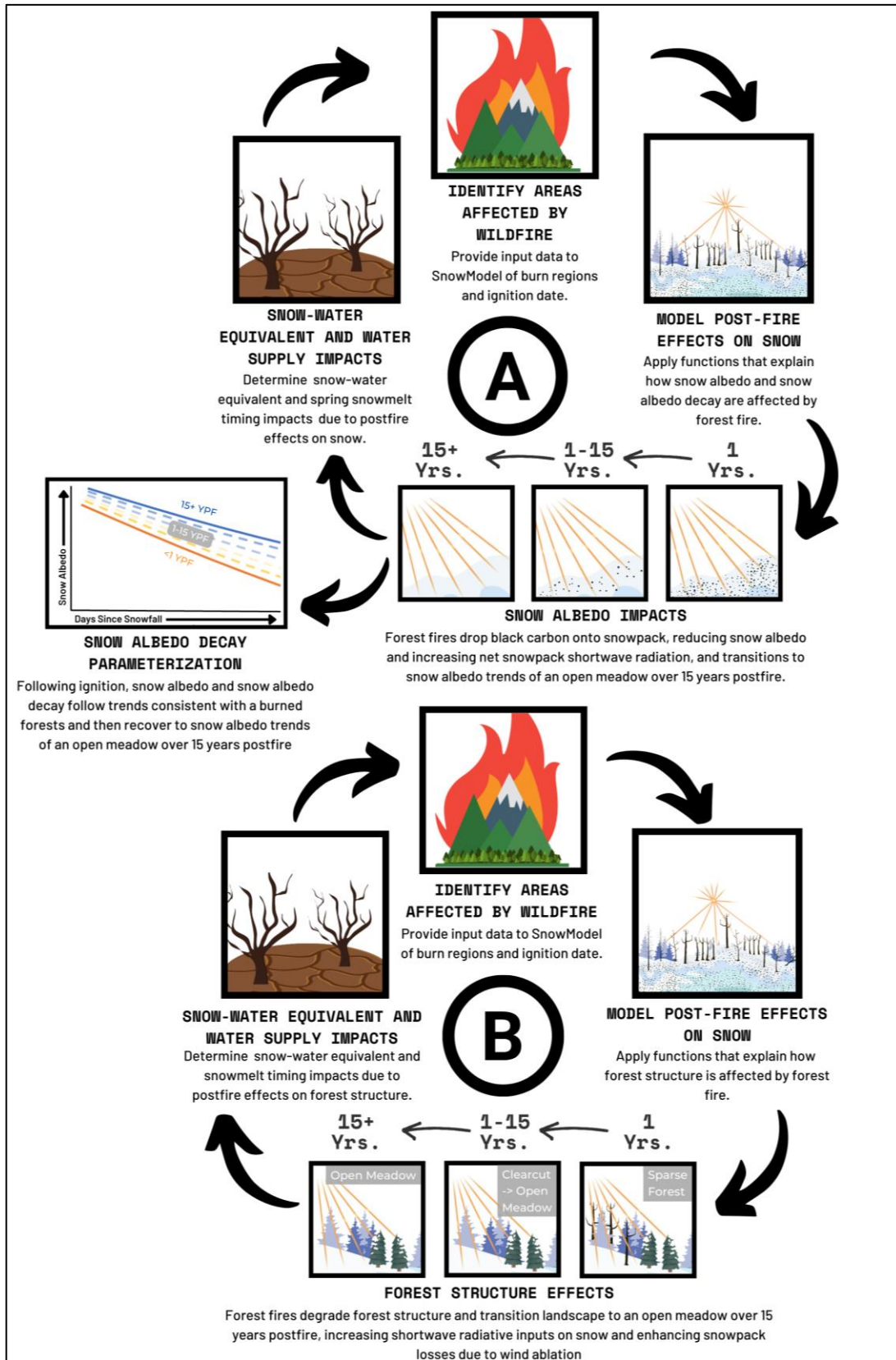


Figure 2: A conceptual model of the postfire snow albedo recovery (A) and postfire forest recovery (B) models.

328 defined in Gleason & Nolin (2016). In burned forests, snow albedo decayed using an exponential
 329 decay coefficient that was adjusted to account for postfire recovery periods over 15 years
 330 following forest fire (Equation 2). Snow albedo in days following fresh snowfall (α_{snow}^{n+1}) is
 331 calculated in the same way as Gleason & Nolin (2016) and Equation 1 except the minimum snow
 332 albedo of a burned forest ($\alpha_{snow,min}$) and the exponential snow albedo decay rate (K_a) are adjusted
 333 by the minimum snow albedo recovery rate ($\Delta\alpha_{snow,min}$) and the snow albedo decay recovery rate
 334 (ΔK_a), respectively, with each rate scaled by the current recovery period (p).

$$335 \quad (\alpha_{snow})^{n+1} = (\alpha_{snow,min} + \Delta\alpha_{snow,min} * p) \\ 336 \quad + ((\alpha_{snow})^n - (\alpha_{snow,min} + \Delta\alpha_{snow,min} * p))^{[-K_a + \Delta K_a * p] * dt} \quad (2)$$

337 To represent the postfire “recovery” of landcover change from burned forest to an open meadow
 338 following fire, the burned forest class snow-holding depths were adjusted by the landcover
 339 recovery rate (ΔSHD) from a scattered conifer forest to a sparse open meadow scaled by the
 340 postfire recovery period (p) using the default values for the endmembers of those landcover
 341 classes included in SnowModel (Equation 3).

$$342 \quad SHD_{burn} = SHD_{forest} - (\Delta SHD * p) \quad (3)$$

343 2.5 Analysis of Model Results

344 2.5.1 Postfire effects on snow-water storage and snow disappearance date

345 Postfire effects on snow hydrology was evaluated by differencing results from the base model
 346 from the results of the postfire snow albedo and forest structure recovery models. Spatially and
 347 temporally integrated forest fire effects on snow-water storage were evaluated by differencing
 348 peak SWE raster for each year in the 20 year modeling period. Peak SWE rasters were created by
 349 determining the maximum SWE for each grid cell for each water year, and differenced from the
 350 base model minus the postfire models, then averaged for burned forest in the chronosequence for
 351 each recovery period following fire. Volumetric changes in peak SWE for each burned forest
 352 were calculated by multiplying the peak SWE differences by the spatial resolution (100 m²),
 353 summing the volumetric differences of each grid cell within each burn region, and then
 354 averaging the total volumetric change in peak SWE.

355 Postfire effects on snow disappearance date (SDD) were quantified by determining the day of
 356 year of snow disappearance for each grid cell for each water year and differencing the postfire
 357 snow albedo or forest structure recovery model results from the base model results. SDD was
 358 defined as the first day following peak SWE in which a grid cell reached zero SWE depth for
 359 each year. Base model annual SDDs were then differenced from the postfire snow albedo
 360 recovery model SDDs and the SDD differences were averaged over the first year postfire, each
 361 three-year bin following fire, and 16+ years postfire according to the ignition date of each fire.

362 2.5.2 Postfire effects on snow hydrology over space, time, and recovery

363 Spatially and temporally integrated and differenced postfire effects snow hydrology metrics were
 364 evaluated monthly including, March 1st to represent accumulation, April 1st to represent the start
 365 of ablation, and May 1st to represent ablation to produce three change in SWE rasters for each

366 date and each year for each fire. The differenced rasters were then averaged in three-year bins for
367 every three years following fire effectively producing a period-averaged March 1st, April 1st, and
368 May 1st differenced raster for each three-year postfire recovery period. The average proportional
369 change in SWE and 95% confidence interval were also calculated for each raster. Daily SWE
370 depth plots were created for each burn over the recovery period to highlight differences in how
371 snow accumulates and melts in forests affected by forest fire over recovery. For each burn, SWE
372 depth values in each pixel were averaged for each daily time-step for all three models. These
373 values were then averaged over period to produce period-averaged SWE for each day of the
374 water year for each recovery period. All calculations were computed using base R (R Core
375 Team, 2021) and the “spatial” package (v7.3-12; Venables & Ripley, 2002). These analyses
376 were performed on all modeled forest fires, but only the results of the Roosevelt forest fire
377 (Ignition Date: 2018) and Green Knoll forest fire (Ignition Date: 2001) were included here as
378 examples illustrating immediate and long-term postfire effects on snow, respectively.

379 2.5.3 Postfire effects on snow hydrology at the watershed scale

380 Watershed scale impacts of postfire effects and recovery on ablation season (May) SWE were
381 investigated within the Lower Granite Creek Hydrologic Unit Code 12 (HUC12) subbasin. We
382 chose to focus on the ablation season for two reasons: 1) postfire effects on snow hydrology were
383 most pronounced following peak SWE and 2) estimations of SWE reductions due to postfire
384 effects would likely be most applicable to watershed managers during the melt season when
385 snowpack is melting off. A United States Geological Survey (USGS) delineation of the
386 watershed was extracted using the Living Atlas tool in ArcGIS (Esri Inc., 2022) and exported
387 into R (U.S. Geological Survey National Geospatial Program, 2022). Annual changes in ablation
388 SWE due to postfire effects were quantified by calculating the average proportional and
389 volumetric difference in SWE within the watershed between both models. Total SWE difference
390 over 20 years between both models was calculated by summing the differences in ablation SWE
391 and converting to volume. Corresponding annual ablation SWE depth rasters from the base
392 model and postfire snow albedo recovery model were differenced, clipped with the watershed
393 delineation file, and plotted using the “spatial” package (v7.3-12; Venables & Ripley, 2002) in
394 R (R Core Team, 2021).

395 2.5.4 Significance testing

396 We tested for statistically significant differences between the base model and postfire snow
397 albedo recovery model using the extracted values of peak SWE, SDD, seasonal SWE (March,
398 April, and May), and watershed SWE. Differences between the base model and postfire snow
399 albedo recovery model results were tested for statistical significance using a two-sided, two-
400 sample Welch t-test using an alpha value of 0.05. All results were analyzed for statistical
401 significance on a subset of paired random samples of 20% of the grid cells within each burn
402 region from the base model and postfire snow albedo and forest structure recovery model rasters
403 and running the t-test using base functions within R (R Core Team, 2021).

404 2.5.5 Model validation

405 Modeled SWE outputs from the base model and postfire snow albedo recovery model were
406 validated using field measurements of SWE taken from six of the modeled burns (Horsethief

407 Canyon, Bull, Boulder, Cliff Creek, Lava Mountain, and Roosevelt) during February and March
408 of 2019 (Figure 1). Prior to validation, the field data were preprocessed using R (R Core Team,
409 2021). Originally, the 114 SWE measurements were collected inside and outside the burn so we
410 first subset the measurements based on measurements that fell within the MTBS burn boundaries
411 of each of the six fires. At each site within the burns, one to three replicates of SWE
412 measurements were taken and, due to the close proximity of the replicates and the modeling
413 resolution of 100 m², replicates were averaged as they always fell within the same modeled
414 pixel. Average measured values were then matched with corresponding modeled SWE results
415 from the base model and postfire snow albedo recovery model using their geographic
416 coordinates and date of collection and the average percentage difference between the values were
417 computed for each fire. An overall average percentage difference was calculated by
418 computing average percentage difference between all observed measurements and the associated
419 base model SWE and postfire snow albedo recovery model SWE.

420 **3 Results**

421 3.1. Summary

422 Postfire reductions in snow albedo and forest structure degradation decreased snow-water
423 storage and advanced snow disappearance date persistently for up to 15 winters following
424 ignition across all modeled forest fires (Table 3). Immediately following fire, snow volume
425 increased slightly during the accumulation period (March 1st), but increased solar forcing from
426 postfire canopy loss and postfire reductions in snow albedo drove earlier melt onset, leading to
427 profound reductions in April and May snow volume (Figure 4). Earlier melt onset resulted in
428 reduced peak snow water volume and earlier SDDs immediately following fire and throughout
429 the 15-year postfire recovery period (Figure 4) with reductions in peak SWE increasing in
430 magnitude 4 to 9 years later (Table 3). Burned forests modeled beyond postfire recovery (>15
431 years postfire) still showed lasting changes in peak SWE and SDD 16+ years following fire
432 (Figure 4; Table 3). At the watershed scale, postfire effects and recovery of three burns modeled
433 in the Lower Granite Creek sub-basin caused net reductions in May 1st SWE in all but one year,
434 with the greatest net reductions in May 1st SWE occurring 3 to 5 years following each burn
435 (Figure 6).

436 3.2. Immediate postfire effects on snow volume and snow disappearance date

437 In the winter immediately following fire, postfire effects decreased peak SWE (-8.42%, sd =
438 9.38%; $p < 0.001$) and advanced SDD by about 5 weeks (34 days, sd = 7 days; $p < 0.001$) on
439 average across all modeled burns (Table 3). Peak SWE shifts one-year postfire varied greatly
440 across burned forests (range of -1.43% to -23.65%) despite their close proximity to one another
441 and identical postfire parameterizations.

442 The Roosevelt forest fire provides an example of postfire effects on snow in the winter
443 immediately following fire. Changes in peak SWE and snow disappearance date in the Roosevelt
444 forest fire were consistent with the changes observed across all modeled forest fires one to three
445 years postfire (peak SWE = -9.34%; $p < 0.001$) and thus the forest fire serves as a good example
446 of both postfire effects on snow in the years immediately following fire and contemporary trends
447 in Western forest fire regimes (Table 3). Over the two winters following the Roosevelt forest

Table 3: Calculations of the differences in volumetric SWE (Snow-Water Equivalent) (<1 year postfire, total, and per period) and differences in snow disappearance date (SDD) between the base model and postfire albedo model. Nearly all modeled fires showed average reductions in peak SWE and advances in SDD relative to the base model in every recovery period following fire. Reductions in peak SWE summed over up to 15 years of recovery were 2 to 18 times greater than the peak SWE losses occurring immediately following fire. In the two burns modeled for the entire 15-year postfire recovery period, peak SWE losses were 7 to 18 times greater than the peak SWE losses 1 year postfire. Over postfire recovery, the greatest losses in peak SWE often did not occur immediately following fire, but instead 4-9 years later. The greatest shifts in SDD tended to occur immediately following fire and then decreased over 15 years following fire with slight fluctuations in this trend. Cells are colored in severity of the change for each burn, with red indicating more severe losses and blue indicating relative gains. The ignition year, total burn area, average elevation, and altitudinal variability for each burn region are included above. Asterisks are also shown on all SWE metrics denoting the level of significant difference between the base model and postfire albedo model (blank: not significantly different, *: $p < 0.05$, **: $0.001 < p < 0.01$; ***: $p < 0.001$).

Burn	Immediate Peak SWE Loss (<1 YPF)	Period 1 (1-3 YPF)	Period 2 (4-6 YPF)	Period 3 (7-9 YPF)	Period 4 (10-12 YPF)	Period 5 (13-15 YPF)	Post-Rec. (16+ YPF)	Total Peak SWE Change (1-15)
Boulder	-7.87%***	-7.64%***/ 4.00%	-5.31%***/ 3.03%	-5.42%***/ 3.54%	-1.06%***/ 7.05%	-2.65%*/ 2.73%	+1.93%***/ 3.16%	-4.13%***
Green Knoll	-16.93%***	-11.93%***/ 4.05%	-14.93%***/ 4.43%	-7.10%***/ 8.28%	-6.67%**/ 3.92%	-6.05%***/ 5.46%	-2.51%***/ 4.12%	-8.09%***
Purdy	-6.28%***	-3.52%***/ 9.69%	+0.30%***/ 11.50%	-2.03%***/ 6.28%	+0.99%***/ 5.20%	+4.48%***/ 7.80%		-0.65%
Bull	-1.43%	-9.23%***/ 5.73%	-5.99%***/ 1.93%	-6.97%***/ 3.36%	-0.08%/ 6.32%			-6.26%***
Horsethief Canyon	-23.65%***	-14.85%***/ 4.73%	-10.97%*/ 5.28%	-6.30%*/ 2.79%				-10.57%***
Lava Mountain	-7.50%***	-6.14%***/ 3.73%	+5.34%***/ 9.16%					-3.60%***
Cliff Creek	-9.11%***	-6.96%*/ 6.39%	-4.27%***/ 11.12%					-6.12%***
Roosevelt	-9.34%***	-6.85%***/ 7.47%						-6.54%***
Avg. Peak SWE Change (%)	8.42%***/ 9.38%	-6.81%***/ 11.23%	-3.14%***/ 13.43%	-3.90%***/ 8.71%	-0.92%***/ 9.37%	+0.86%***/ 9.82%	-0.30%***/ 4.29%	-4.46%***/ 11.43%
Avg. Peak SWE Change (m ³)	-4.34M***/ 5.03M	-8.13M***/ 7.49M	-1.78M***/ 1.77M	-2.27M***/ 1.19M	-0.16M***/ 1.31M	+0.64M***/ 2.95M	-0.09M***/ 0.34M	-10.96M***/ 7.02M
Avg. SDD Shift (days)	-34 days***/ 7 days	-31 days***/ 9 days	-27 days***/ 13 days	-22 days***/ 8 days	-17 days***/ 6 days	-8 days***/ 6 days	-5 days***/ 6 days	

448 fire (2019 and 2020), average March 1st SWE increased ($6.93 \pm 1.21\%$, $p = 0.017$) driven
 449 primarily by the more open postfire forest canopy (Figure 3a) with postfire snow albedo
 450 reductions causing a minimal net increase in solar shortwave inputs (Figure 5a). Average April
 451 1st SWE in the postfire snow albedo recovery model was not significantly different than in the
 452 base model, indicating that the increase in March 1st SWE observed earlier was lost, primarily
 453 due to earlier melt onset from postfire effects on snow albedo (Figure 3b and Figure 5a).
 454 Following April 1st, melt onset began in earnest in the postfire snow albedo recovery model
 455 while snow continued to accumulate until mid to late April in the base model and postfire forest
 456 structure model (Figure 3d), an indication that earlier melt onset was primarily driven by postfire
 457 effects on snow albedo. By May 1st, average snowpack volume within the Roosevelt burned
 458 forest had decreased significantly ($-45.76 \pm 27.41\%$, $p < 0.001$) in the postfire snow albedo
 459 recovery model as a result of the earlier melt onset and decreased average peak SWE (Figure 3c).
 460 Earlier melt onset and decreased average peak SWE in the Roosevelt burn then culminated in a

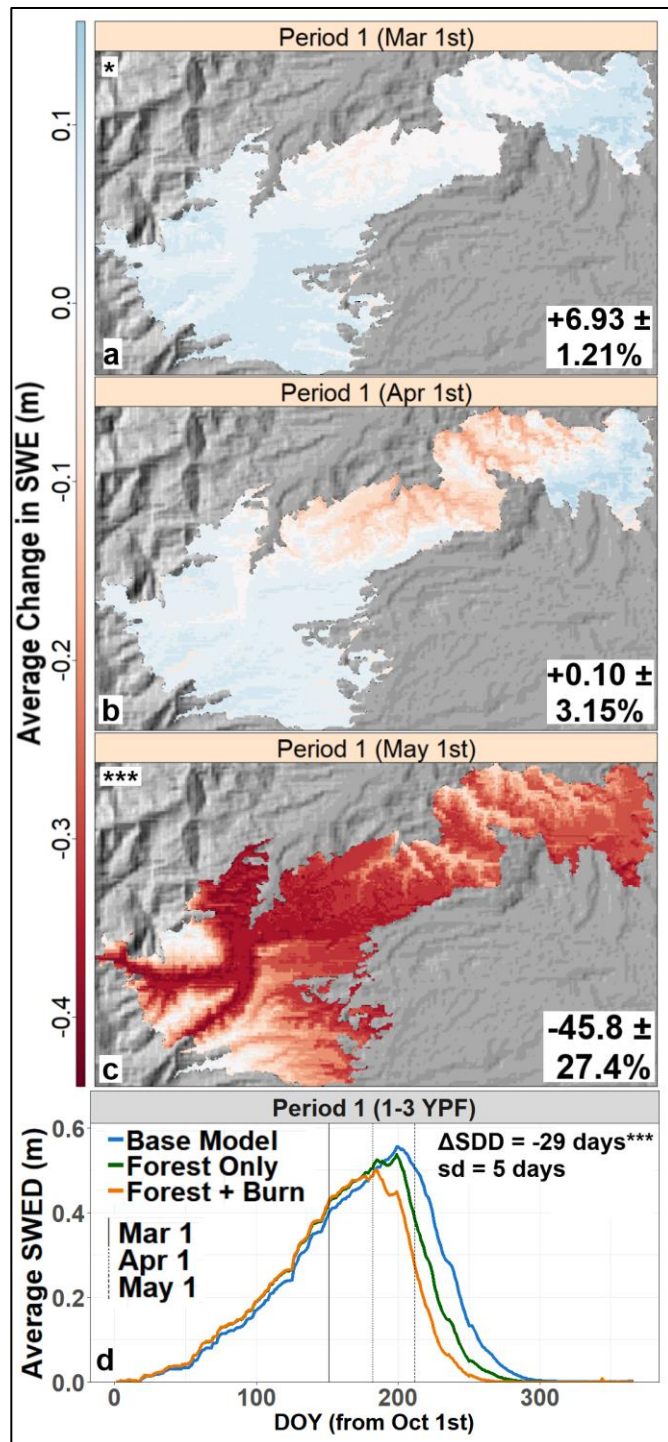


Figure 3: Change in snow-water equivalent (SWE) depth between the base model and postfire snow albedo recovery model in Roosevelt forest fire (Ignition Year: 2018). Postfire effects caused small increases in average March 1st SWE (a), no significant difference in average April 1st SWE (b), and large reductions in average May 1st SWE (c) across the burn region. Prior to April 1st, the average SWE of the postfire forest and postfire albedo model was greater than the base model (d).

29-day earlier average snow disappearance date (sd = 5 days; $p < 0.001$) over the full data record for the Roosevelt Fire of two years following fire (Table 3).

3.3. Recovery of postfire effects on snow volume and snow disappearance date

Postfire effects on snow albedo and forest structure steadily recovered over 15 years following fire, yet subsequent changes in peak SWE and SDD did not follow the same trend. Average postfire reductions in peak SWE tended to decrease in magnitude from 1 to 6 years postfire (-6.81% to -3.14%; $p < 0.001$) but increased in magnitude 4 to 9 years postfire, with this increase occurring in most fires 7 to 9 years postfire (-3.14% to -3.90%; $p < 0.001$) (Table 3). Across all burns, peak SWE reductions were also most variable in this same period (4-6 YPF: sd = 13.43%). Despite identical parameterizations across each burn and averaging over across time and climatology, changes in snow hydrology were still highly variable 4-6 years postfire and suggesting that diversity in landscape and elevation was responsible for much of the variability in postfire snow hydrology.

The Green Knoll forest fire provides an example of the long-term recovery of postfire effects on snow. In the Green Knoll forest fire, the greatest reductions in peak SWE over postfire recovery did not occur immediately following fire, but instead 4-6 years postfire (-14.93%, sd = 4.43%, $p < 0.001$) (Table 3). Over 15 years of postfire recovery, postfire effects on snow albedo and forest structure in the Green Knoll burn caused small increases and decreases in accumulation season SWE 1 to 15 years postfire (range: -1.60% ± 5.75% to +7.13% ± 12.93%, $p < 0.001$; Figure 4a). Accumulation period SWE (March 1st SWE) averaged over period was

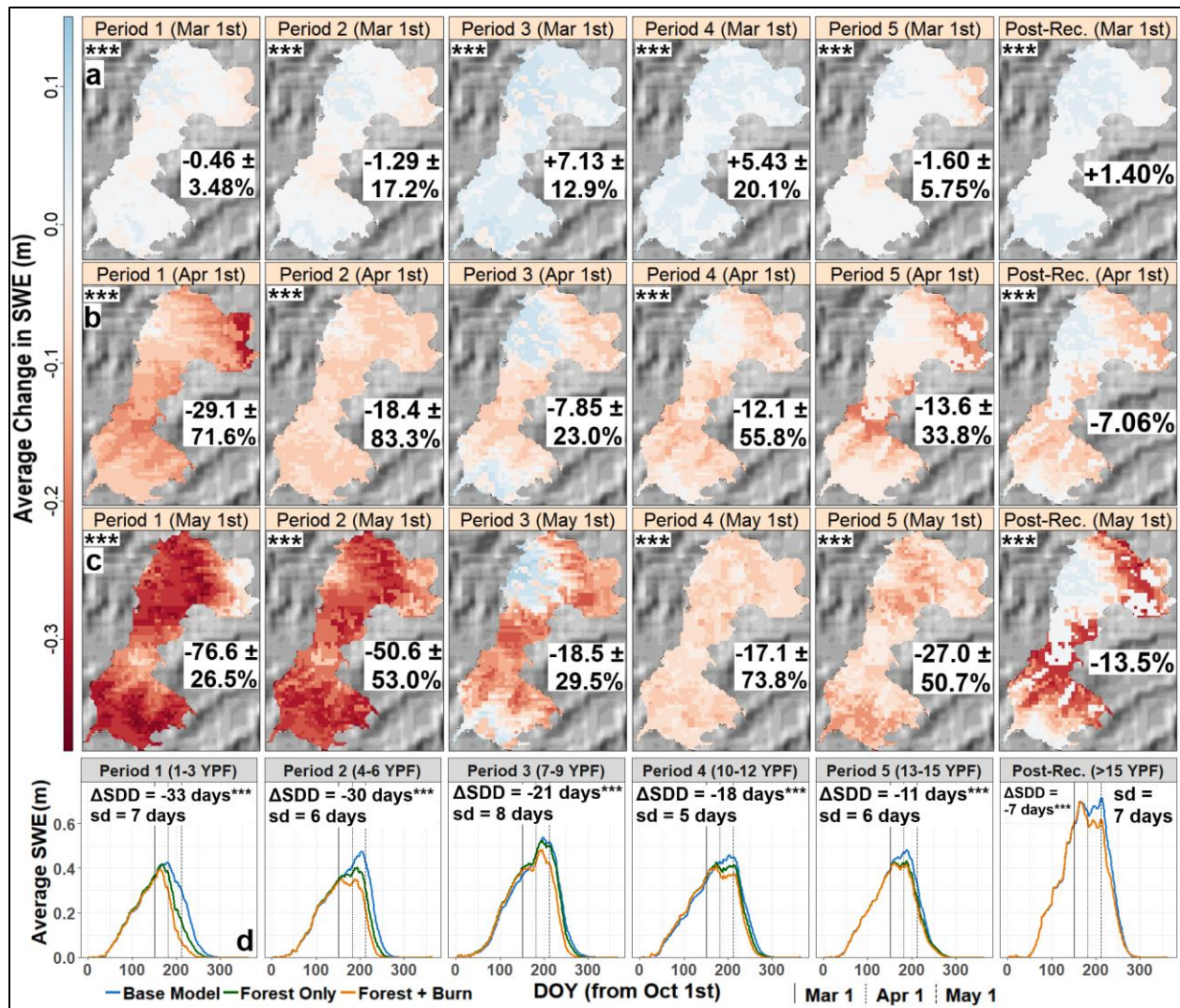


Figure 4: The change in snow-water equivalent depth (SWE) depth between the base model and postfire snow albedo recovery model in the Green Knoll fire (Ignition Year: 2001). Over 15 years of postfire recovery, postfire effects caused slight changes in SWE during March 1st (a), but then caused modest reductions in April 1st SWE (b), followed by profound reductions in May 1st (c). Postfire changes in SWE tended to reduce in magnitude over each successive recovery period, but, critically, post-recovery reductions in SWE were still present 16+ years following fire (d).

505 similar between the postfire snow albedo recovery model and postfire forest structure model for
 506 all recovery years, indicating that accumulation patterns over recovery were likely driven by
 507 postfire effects on forest structure and that postfire effects on snow albedo play a smaller role in
 508 affecting snow accumulation during this period (Figure 4d). Average reductions in SWE in the
 509 postfire snow albedo recovery model began to manifest during April and May of each winter 1 to
 510 15 years following fire. Start of ablation SWE (April 1st SWE) decreased in the postfire snow
 511 albedo recovery model relative to the base model across the 16+ year recovery period (range: -
 512 29.12% ± 71.64% to -7.85% ± 23.01%) with significant reductions occurring 1-6 years postfire
 513 and 10-12 years postfire ($p < 0.001$) (Figure 4b). Snowmelt period SWE (May 1st SWE)
 514 profoundly decreased in the postfire snow albedo recovery model across the recovery period (1
 515 to 15 years postfire) (range: -76.63% ± 26.47% to -17.05% ± 73.76%), with significant average

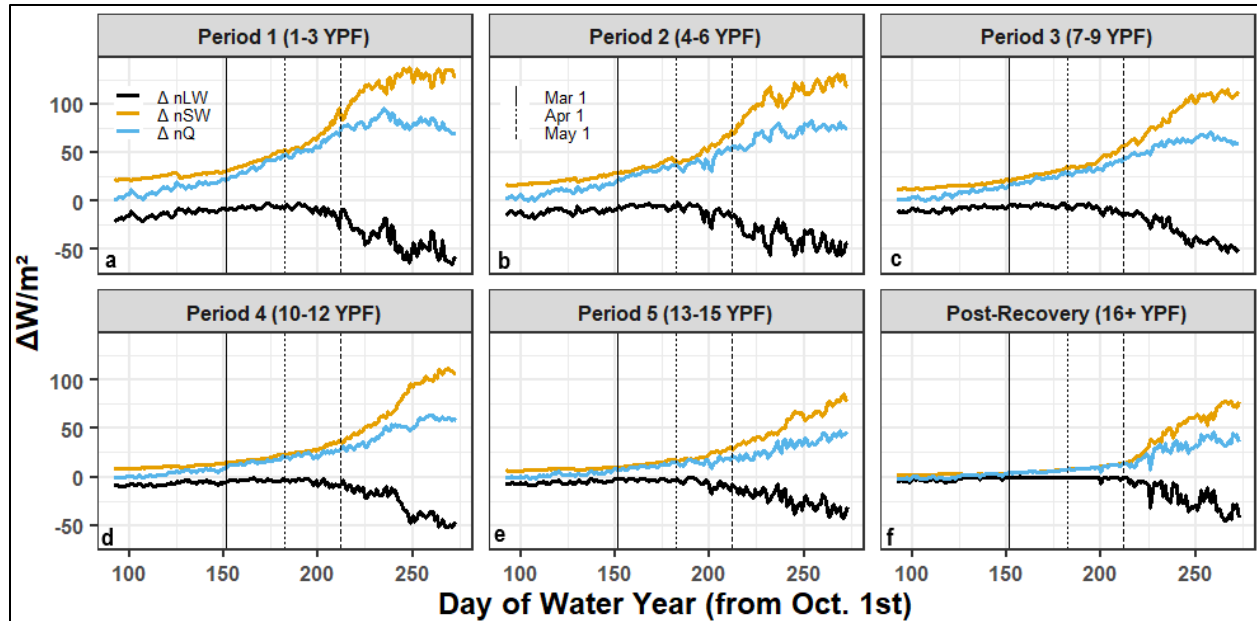


Figure 5: Difference between base model and postfire albedo model net components of the snowpack energy balance averaged over 3-year bins since burn. The progressively more open postfire canopy allowed for increased solar shortwave incident on the snow surface over years since fire, but increasing snow albedo over years since fire drive the increases in internal snowpack energy and associated changes in snowpack volume. The difference in net shortwave inputs between models decreases over years since fire showing that postfire effects on snow albedo drive changes in peak snowpack volume over 15 years postfire and beyond.

516 reductions occurring in all years except 7-9 years postfire ($p < 0.001$) (Figure 4c). SWE
 517 reductions present in April and May reflect the postfire shift to earlier melt onset which tended to
 518 occur prior to April 1st for all years 1-15 years postfire (Figure 4d). Average SWE in the postfire
 519 snow albedo recovery model began to diverge from the postfire forest structure model during
 520 peak SWE (April 1), (1 to 12 years postfire), with the postfire forest structure model continuing
 521 to accumulate snow beyond April 1st (Figure 4d). Alterations in the snowpack energy balance
 522 during this period were dominated by additional shortwave solar inputs (Table A2-A3; Figure 5).
 523 Additional shortwave radiative forcing due to postfire degradation of forest canopy accounted for
 524 the majority of added inputs relative to postfire effects on snow albedo (54.0-18.9% vs. 29.2-
 525 0.00%) (Figure A1-2; Figure 5).

526 Snow disappearance date advanced by a month immediately following fire and earlier snow
 527 disappearance persisted across all postfire recovery years (1-15 years postfire) in the postfire
 528 snow albedo-forest model, with the greatest advances in SDD occurring 1-3 years postfire (-31
 529 days, $sd = 9$ days; $p < 0.001$) (Table 3). Even after 15 years following fire SDD remained 5 days
 530 earlier in the postfire snow albedo and forest recovery models than the base model, due to the
 531 postfire landcover recovering from burned forest to open meadow after 15 years following fire.
 532 Advances in SDD decreased over the 15 year postfire recovery period evaluated, with slower
 533 recovery between 1 to 12 years postfire (14 days over 12 years) and rapid recovery 12 to 15
 534 years postfire (9 days over 3 years) (Table 3).

535 In total, postfire effects on peak SWE summed over 15 years of postfire recovery and averaged
 536 across all burns amounted to a total reduction in snow volume of $10.96M m^3$ ($sd = 7.02M m^3$; p
 537 < 0.001) or 4.46% reduction ($sd = 11.43\%$; $p < 0.001$), double the loss in snow volume

538 immediately in the 1st year postfire ($4.85\text{M m}^3/8.42\%$; $\text{sd} = 5.03 \text{ m}^3/9.38\%$; $p < 0.001/p < 0.001$)
539 (Table 3). In the post-recovery period (16+ years postfire), peak SWE still was reduced in the
540 Green Knoll burn region (-2.51% , $\text{sd} = 4.12\%$; $p < 0.001$) (Table 3). Post-recovery, accumulation
541 period (March 1st) SWE increased by $+1.40\%$ ($p < 0.001$) on average (Figure 4a), while peak
542 SWE and snowmelt period (April and May) SWE was still reduced due to the post recovery
543 shift in snow albedo and forest parameterizations to open meadow (April: -7.60% , $p < 0.001$;
544 May: -13.50% , $p < 0.001$) (Figure 4b-c). During this period, recovery of changes in the
545 snowpack energy balance were primarily attributed to changes in net shortwave energy (Figure
546 5f; Table A3) and these changes in net shortwave energy were primarily driven by increases in
547 outgoing shortwave (Figure A1f). Thus, the recovery of peak SWE was primarily driven by the
548 recovery of snow albedo occurring from the transition of postfire forest to an unburned open
549 meadow rather than due to changes in forest canopy degradation over the same transition (Figure
550 A1f; Figure 5f).

551 3.4. Effects of postfire impacts and recovery at the watershed scale

552 Integrating forest fire effects on snow albedo and forest structure recovery across the subbasin
553 showed long-lasting and persistent reductions in snow-water storage at the watershed scale
554 particularly in the ablation period (May). Here, we focus on postfire effects on snow hydrology
555 during the ablation period as 1) postfire effects on snow albedo and forest structure caused the
556 greatest reductions in snow water storage at the watershed scale in the ablation period and 2)
557 estimations of postfire effects on snowmelt timing and volume during ablation have greater
558 applicability to watershed hydrology and watershed management . Three of the modeled forest
559 fires (Boulder, Bull, and Roosevelt) occurred entirely or partially within the Lower Granite
560 Creek (LGC) subbasin. The Boulder forest fire was the earliest occurring burn (2000) and took
561 place entirely within the LGC subbasin (15 km^2 ; 13.05% of the watershed area), while the Bull
562 and Roosevelt fires occurred partially within the LGC subbasin (burning 12 km^2 [10.48%] and 23
563 km^2 [19.81%] of the basin, respectively) (Figure 6). In combination, all three fires burned
564 43.37% of the watershed area over the 20-year modeling period (50.45 km^2) (Figure 6).

565 Forest fires in the LGC subbasin largely caused annual losses in ablation season snow volume
566 over 20 years (average $6.30 \pm 6.95\%$ loss in May 1st SWE) with the greatest proportional losses
567 in SWE occurring during 2015 and 2019 ($-9.50 \pm 68.0\%$ and $-14.58 \pm 76.1\%$; $p < 0.001$) (Figure
568 6). During 2015, postfire effects from both the Boulder and Bull forest fires impacted snow
569 volumes within the LGC subbasin (both burns occurred <15 years prior) and, combined, caused a
570 $9.50 \pm 68.80\%$ reduction in May 1st SWE ($p < 0.001$). During 2019, postfire impacts from the
571 Cliff Creek burn (occurring 3 years prior) caused a 14.58% reduction in May 1st SWE in
572 combination with the postfire recovery effects from the Bull forest fire (occurring 9 years prior)
573 (Figure 6; 2012 and 2019). Forest fires relatively late in their postfire recovery continued to
574 cause losses and enhanced immediate losses from more recent burns. Repeated burns within the
575 LGC subbasin and the associated postfire impacts on snow and forest structure resulted in a total

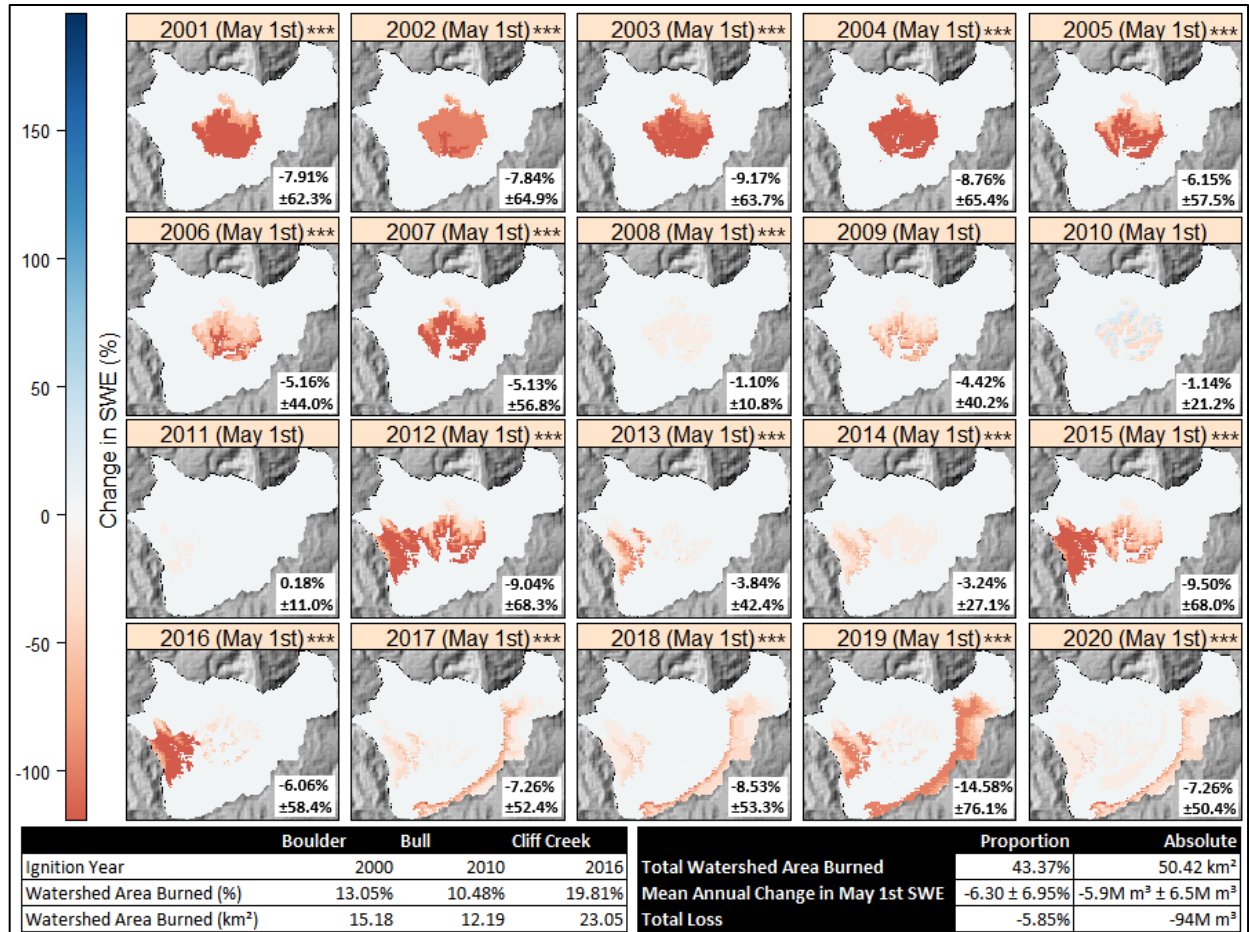


Figure 6: Watershed scale impacts of postfire effects and recovery in the Lower Granite Creek (LGC) subbasin during the ablation period (May 1st) for every year in the simulation. Postfire effects on snow albedo and forest structure caused net reductions in average May 1st SWE within the LGC subbasin in all but one year between 2000 and 2020, indicating that postfire effects on snow and forest structure cause lasting reductions in watershed-scale ablation season SWE for many years following fire. Further, the greatest losses in May 1st SWE did not occur immediately following each burn, but instead 3 to 5 years afterwards.

576 reduction of 5.85% in May 1st SWE over the 20-year modeling period, a total volume of >94M
 577 m³ of additional snowmelt by May 1st (Figure 6).

578 3.5 Model Validation

579 Based on our validation of the modeled results using in-situ SWE measurements collected from
 580 within several of the burn regions, we overestimated SWE in both the base model (+40.22 ±
 581 38.88%) and postfire snow albedo recovery model (+41.61 ± 46.29%) and both models were
 582 relatively close in accuracy (<1.5% difference). Both the base model and postfire snow albedo
 583 recovery model overestimated SWE in the individual fires and, again, showed similar levels of
 584 accuracy between one another (Table 4).

585 4 Discussion

586 Improved modeling of forest fires effects on snow albedo and forest structure incorporating
 587 postfire recovery allowed for volumetric watershed scale estimates of postfire reductions in

Table 4: Results of the model validation using field measurements of SWE collected from six of the burns between February and March of 2019. Percent error between the base/postfire albedo model were calculated against the field observations and the standard deviation was included when $n > 1$. Instances where the postfire snow albedo model performed better than the base model are in bold.

Fire	Base Model		Postfire Snow Albedo Model		n
	Avg. % Error (%)	SD (%)	Avg. % Error (%)	SD (%)	
Horsethief Canyon	+61.06	-	+58.64	-	1
Bull	+24.67	16.62	+23.03	16.9	16
Boulder	+40.71	11.02	+41.22	11.15	9
Cliff Creek	+40.4	13.47	+41.17	9.765	13
Lava Mountain	+48.89	12.04	+46.18	15.13	8
Roosevelt	+59.79	13.42	+67.89	11.96	13
Overall	+40.22	19.44	+41.61	23.15	60

588 snow-water storage and snow persistence. Peak snow-water storage decreased by ~4.5% and
 589 snow disappearance date advanced by over a week for at least 15 years following fire (Table 3).
 590 Sustained shifts in snow-water storage and snow-off date have the capacity to advance the timing
 591 of peak streamflow (Wieder et al., 2022), reduce spring and summertime soil moisture (Harpold,
 592 2016; Westerling, 2016), extend growing seasons, and increase risk of future forest fire for many
 593 years beyond ignition (Abatzoglou & Kolden, 2013; Westerling, 2016). Our estimates discussed
 594 here highlight the importance of incorporating postfire effects on snow hydrology and can help
 595 to inform management of threatened water resources and forest fire mitigation in burned
 596 montane watersheds similar to our study region.

597 4.2. Immediate postfire effects on snow hydrology

598 Immediately following fire, postfire effects reduce snow-water storage by >8% and advance
 599 snow disappearance date by as much as 34 days (Table 3). These changes are primarily due to
 600 earlier melt onset from darkened postfire snow albedo (Figure A2; Figure 5) and become evident
 601 at or beyond the timing of peak snow-water storage (Figure 3c-d). Although increases in snow
 602 accumulation in March due to postfire forest structure degradation buffer later reductions in
 603 snow-water storage, these increases are ultimately overcome by profound reductions in snow-
 604 water storage between April and May (Figure 3d). Most of the reductions in snow-water storage
 605 due to postfire effects occur later in the snow season immediately following fire as insolation
 606 increases, temperatures warm, and postfire effects from darkened snow albedo become more
 607 pronounced (Figure 3c-d). Further, our estimates indicate that snowpack in burned forests
 608 disappears about one month earlier on average in the year immediately following fire (-34 days,
 609 $sd = 7$ days) and that this earlier disappearance is related to the advanced timing of snowmelt
 610 onset. Estimates of snow-water storage in burned montane forested watersheds made around the
 611 time of historical peak snow-water storage may not be adequate for accurate hydrological
 612 forecasting of snow-water reserves available later in the year as our estimates show the most
 613 profound postfire effects on snow-water storage occur later in the snow season.

614 4.3. Recovery of postfire effects on snow hydrology

615 Snow-water storage in burned forests largely shrank on average for the entire 15 year postfire
 616 recovery period (Table 3). Earlier melt onset advanced snow disappearance dates occurred in all
 617 modeled burns over all recovery periods (-31 to -8 days) and even post-recovery (16+ years

618 postfire: -5 days). Reductions in snow-water storage and earlier snow disappearance have been
619 shown to drive decreases in minimum stream flows (Godsey et al., 2014; Hallema et al., 2018),
620 lengthened growing seasons and the likelihood of spring and summertime water stress (Harpold,
621 2016; Westerling, 2016), and the occurrence, severity and extent of early season forest fire
622 (Abatzoglou & Kolden, 2013; Westerling, 2016).

623 Although advances in snow disappearance dates and reductions in peak snow-water storage
624 decreased on average over years since fire (Table 3), snowpack within burned forests showed
625 widely varying responses in snow disappearance date timing ($6 \text{ days} \leq \text{sd}(\Delta\text{SDD}) \leq 13 \text{ days}$) and
626 peak snow-water storage reductions ($8.71\% \leq \text{sd}(\Delta\text{SWE}) \leq 11.12\%$) over postfire recovery.
627 These results highlight the difficulty in predicting the degree to which snow-water storage will
628 be affected in burned watersheds over many years following fire, despite uniform
629 parameterizations across each forest fire and a narrow scope of landscape and climate variability
630 contained within the study region. Regions in the western United States rely on predictable
631 spring runoff afforded by ample snow-water storage. Such variability in postfire snow hydrology
632 responses within our relatively narrow scope of study compound with spatial and climactic
633 variability across the western United States and increasing interannual variability in runoff
634 timing due to the effects of climate change on snow-water storage and snowmelt timing (Li et al.,
635 2017; Wieder et al., 2022).

636 Over the 15 years of postfire recovery, snow albedo and forest structure recovered from that of a
637 recently burned forest towards an unburned open meadow as observed in Gersh et al (2022). Our
638 parameterizations improved upon those of Gleason and Nolin (2016) by extending the
639 parameterization of postfire snow hydrology immediately following fire to the recovery of snow
640 albedo and forest structure over 15 years following fire. The results covered here provide
641 evidence that snowpack in burned forests still exhibits reductions in peak snow-water storage (-
642 0.30%, $\text{sd} = 4.29\%$) and earlier snow disappearance date (-5 days, $\text{sd} = 6 \text{ days}$) 16 years postfire
643 and beyond (Table 3). Future parameterizations need to be extended to capture the full postfire
644 recovery through regeneration to prefire conditions or other altered postfire states in order to
645 calculate estimates of the complete effect of forest fire on snow hydrology.

646 4.4. Postfire effects on snow hydrology at the watershed scale

647 Watershed scale postfire effects reduced snow water storage and advanced snowmelt timing
648 during the snowmelt period (May) across the 20 year modeling period (Figure 6). Postfire effects
649 on snow albedo and forest structure from the Boulder, Bull and Cliff Creek fires caused annual
650 reductions in May 1st snow volume within the Lower Granite Creek subbasin in all but one year
651 (2011) of the 20-year modeling period (Figure 6). Trends in the recovery of postfire effects on
652 May 1st SWE held at the watershed scale, with the greatest reductions in snow volume due to
653 postfire effects occurring 3 to 5 years following each forest fire, rather than in the year
654 immediately following each burn. Earlier snowmelt onset and peak snow-water storage caused
655 by these forest fires led to earlier average annual snowmelt of $5.9\text{M m}^3 \pm 6.5\text{M m}^3$ per year and,
656 over 20 years, resulted in a total of $>94\text{M m}^3$ of added early snowmelt than would occur in no-
657 burn conditions. As a frame of reference, the USGS stream gauge at the outlet of the Lower
658 Granite Creek sub-basin (USGS 13019438) measured an annual average streamflow volume of
659 29M m^3 per year between 1982 and 1993 (USGS, 2022). However, it is likely these calculations
660 are underestimating the full extent of postfire effects on snow albedo and forest structure over

661 postfire recovery. Reductions in May 1st SWE were still visible as late as 2020 in the Boulder
662 burn region, 4 years following the end of the postfire recovery period and postfire effects from
663 the Bull (Ignition Date: 2010) and Cliff Creek fire (Ignition Date: 2016) were not captured over
664 the extent of the full 15-year postfire recovery period (Figure 6).

665 As forest fires across the western United States become more frequent and extensive, how forest
666 fire affects snow-water resources at the watershed scale and over many years following fire
667 becomes an increasingly critical question. Multiple studies have demonstrated that reductions in
668 peak snow volume can alter summer low flows (Godsey et al., 2014; Jenicek et al., 2018),
669 especially in cold and dry continental snow zones (Hammond et al., 2018), and that annual river
670 flow can be altered in watersheds burned for as little as 19% of their area (Hallema et al., 2018).
671 The changes in peak snow-water storage due to postfire effects on snow hydrology modeled here
672 have the capacity to alter resulting annual streamflow runoff (Godsey et al., 2014). Our findings
673 provide the first three-dimensional, spatially-distributed, time varying, process-based estimates
674 of postfire effects on snow hydrology and recovery over many years following fire and provide a
675 basis for future estimates of associated effects on the timing and volume of spring streamflow.

676 4.5. Model validation

677 Both the base model and postfire albedo model overestimated SWE (+40.22%, sd = 19.44% vs.
678 +41.61%, sd = 23.20%) in the individual fires and showed similar levels of accuracy between
679 one another (Table 4). However, the field validation data for each burn were collected within
680 close proximity to one another over the course of ~5 weeks in a single year while the modeled
681 results span multiple decades and thousands of square kilometers, calculated in grids of 100 m².
682 Although the model tended to overestimate SWE at the field validation sites, the model showed
683 good agreement with 20 years of continuous data from SNOTEL sites spatially-distributed across
684 the study region (Table 2) lending support for the estimates of postfire effects on snow over the
685 broad spatial and time scales investigated in this study.

686 4.6. Uncertainties in modeling postfire effects on snow albedo and forest structure

687 We employed a postfire snow albedo and snow albedo decay parameterization developed in the
688 Oregon Cascades to model postfire effects on snow hydrology in the Rocky Mountains
689 introducing key uncertainties in how postfire effects on snow hydrology might differ between
690 these two disparate snow climates and the associated influence on our results. However, research
691 by Gleason & Nolin (2016) was the only published parameterization of postfire effects on snow
692 albedo and snow albedo decay at the time of publication and thus it is uncertain how postfire
693 effects on snow albedo might differ across these two snow climates. In addition, our
694 parameterization of postfire forest structure modeled recovery in a simplified, linear fashion
695 while previous work investigating postfire effects on forest structure in similar regions shows
696 that delayed tree mortality can occur at an exponentially decaying rate following fire (Angers et
697 al., 2011; Brown & DeByle, 1987) and can depend on many factors such as seed supply, distance
698 to sources, and pre- and postfire climate (Stevens-Rumann & Morgan, 2019). The modeling
699 capabilities of forest structure dynamics in the current iteration of SnowModel are limited, but

700 future expansions of SnowModel will allow for more precise estimates of postfire effects on
701 forest structure and recovery and the resulting effects on snow hydrology.

702 **5 Conclusions**

703 Forest fire darkens snow albedo and degrades forest structure, increasing radiative forcing on
704 snow for years following fire, and carrying with it the capacity to significantly alter snow
705 evolution and, by extension, water supply over multi-decadal time scales. This study assessed the
706 long-term water supply impacts of postfire effects on snow hydrology by incorporating an
707 improved postfire snow albedo and forest structure recovery parameterization in a snow mass
708 and energy balance model and estimating postfire effects on snow albedo and forest structure and
709 recovery on peak SWE, SDD, and SWE volume reductions.

710 Immediately following forest fire, snowpack storage increased by up to 6.93% in early winter,
711 but decreased by 8.43% during spring and up to 87.97% by May with earlier melt onset and 30+
712 day advanced snow disappearance. Following a 15 year postfire recovery period, burned forests
713 still exhibited reduced peak snow-water storage of 0.30% and a 5 day earlier snow
714 disappearance date due to the shift from forest to open meadow. Forest fires effects within the
715 burned perimeter integrated over 15 years following fire amounted to an average 4.5% reduction
716 on snow-water storage.

717 Watershed scale forest fire effects on snow-water storage and snowmelt are persistent for
718 decades following fire. The results of this study show that forest fire has immediate, profound,
719 and lasting effects on snow hydrology and water supply that last decades beyond the initial burn
720 event and have hydrological implications beyond the forest fire perimeter. Quantification of
721 changes in snow volume and snow melt on the snow-mass energy- balance using process-based
722 snow models provide information critical to our understanding of the long-term impacts of an
723 increasingly severe fire regime on the quantity and timing of freshwater originating from
724 springtime snowmelt.

725 **Acknowledgments**

726 This research was funded by NASA as part of the Terrestrial Hydrology Program (Award
727 #80NSSC19K0002). Special thanks to Glen Liston for his support in running SnowModel and
728 troubleshooting our modifications and to Ryan Crumley for his support in initializing
729 SnowModel.

730 **Open Research**

731 All data used to produce the results of this study including model inputs, model outputs, and
732 SnowModel parametrization files are available through PDX Scholar at [Temporary link via
733 Google Drive:

734 [https://drive.google.com/drive/folders/1exRuIPaU4sAqAHp3sJewWTch_WNMpe_T?usp=shari](https://drive.google.com/drive/folders/1exRuIPaU4sAqAHp3sJewWTch_WNMpe_T?usp=sharing)
735 [ng](https://drive.google.com/drive/folders/1exRuIPaU4sAqAHp3sJewWTch_WNMpe_T?usp=sharing)].

736

737 **References**

- 738 Abatzoglou, J. T., & Kolden, C. A. (2013). Relationships between climate and macroscale area
739 burned in the western United States. *International Journal of Wildland Fire*, 22(7), 1003.
740 <https://doi.org/10.1071/WF13019>
- 741 Angers, V. A., Gauthier, S., Drapeau, P., Jayen, K., & Bergeron, Y. (2011). Tree mortality and
742 snag dynamics in North American boreal tree species after a wildfire: A long-term study.
743 *International Journal of Wildland Fire*, 20(6), 751. <https://doi.org/10.1071/WF10010>
- 744 Armitage, R. P., Alberto Ramirez, F., Mark Danson, F., & Ogunbadewa, E. Y. (2013).
745 Probability of cloud-free observation conditions across Great Britain estimated using
746 MODIS cloud mask. *Remote Sensing Letters*, 4(5), 427–435.
747 <https://doi.org/10.1080/2150704X.2012.744486>
- 748 Barnett, T. P., Adam, J. C., & Lettenmaier, D. P. (2005). Potential impacts of a warming climate
749 on water availability in snow-dominated regions. *Nature*, 438(7066), 303–309.
750 <https://doi.org/10.1038/nature04141>
- 751 Brown, J. K., & DeByle, N. V. (1987). Fire damage, mortality, and suckering in aspen. *Canadian*
752 *Journal of Forest Research*, 17(9), 1100–1109. <https://doi.org/10.1139/x87-168>
- 753 Brown, O. L. I. (1951). The Clausius-Clapeyron equation. *Journal of Chemical Education*, 28(8),
754 428. <https://doi.org/10.1021/ed028p428>
- 755 Buchhorn, M., Smets, B., Bertels, L., Roo, B. D., Lesiv, M., Tsendbazar, N.-E., Li, L., & Tarko,
756 A. (2020). *Copernicus Global Land Service: Land Cover 100m: version 3 Globe 2015-*
757 *2019: Product User Manual* (Dataset v3.0, doc issue 3.3). Zenodo.
758 <https://doi.org/10.5281/ZENODO.3938963>

- 759 Campagnolo, M. L., Sun, Q., Liu, Y., Schaaf, C., Wang, Z., & Román, M. O. (2016). Estimating
760 the effective spatial resolution of the operational BRDF, albedo, and nadir reflectance
761 products from MODIS and VIIRS. *Remote Sensing of Environment*, *175*, 52–64.
762 <https://doi.org/10.1016/j.rse.2015.12.033>
- 763 Cescatti, A., Marcolla, B., Santhana Vannan, S. K., Pan, J. Y., Román, M. O., Yang, X., Ciais,
764 P., Cook, R. B., Law, B. E., Matteucci, G., Migliavacca, M., Moors, E., Richardson, A.
765 D., Seufert, G., & Schaaf, C. B. (2012). Intercomparison of MODIS albedo retrievals and
766 in situ measurements across the global FLUXNET network. *Remote Sensing of*
767 *Environment*, *121*, 323–334. <https://doi.org/10.1016/j.rse.2012.02.019>
- 768 Danielson, J. J., & Gesch, D. B. (2010). *Global Multi-resolution Terrain Elevation Data 2010*
769 *(GMTED2010)*.
- 770 Esri Inc. (2022). *2D, 3D & 4D GIS Mapping Software | ArcGIS Pro*. [https://www.esri.com/en-](https://www.esri.com/en-us/arcgis/products/arcgis-pro/overview)
771 [us/arcgis/products/arcgis-pro/overview](https://www.esri.com/en-us/arcgis/products/arcgis-pro/overview)
- 772 Finco, M., Quayle, B., Zhang, Y., Lecker, J., Megown, K. A., & Brewer, C. K. (2012).
773 Monitoring Trends and Burn Severity (MTBS): Monitoring wildfire activity for the past
774 quarter century using landsat data. In: *Morin, Randall S.; Liknes, Greg C., Comps.*
775 *Moving from Status to Trends: Forest Inventory and Analysis (FIA) Symposium 2012;*
776 *2012 December 4-6; Baltimore, MD. Gen. Tech. Rep. NRS-P-105. Newtown Square, PA:*
777 *U.S. Department of Agriculture, Forest Service, Northern Research Station. [CD-ROM]:*
778 *222-228., 222–228.*
- 779 Gersh, M., Gleason, K. E., & Surunis, A. (2022). Forest Fire Effects on Landscape Snow Albedo
780 Recovery and Decay. *Remote Sensing*, *14*(16), 4079. <https://doi.org/10.3390/rs14164079>

- 781 Gleason, K. E., McConnell, J. R., Arienzo, M. M., Chellman, N., & Calvin, W. M. (2019). Four-
782 fold increase in solar forcing on snow in western U.S. burned forests since 1999. *Nature*
783 *Communications*, 10(1), 2026. <https://doi.org/10.1038/s41467-019-09935-y>
- 784 Gleason, K. E., & Nolin, A. W. (2016). Charred forests accelerate snow albedo decay:
785 Parameterizing the post-fire radiative forcing on snow for three years following fire.
786 *Hydrological Processes*, 30(21), 3855–3870. <https://doi.org/10.1002/hyp.10897>
- 787 Gleason, K. E., Nolin, A. W., & Roth, T. R. (2013). Charred forests increase snowmelt: Effects
788 of burned woody debris and incoming solar radiation on snow ablation: CHARRED
789 FORESTS INCREASE SNOWMELT. *Geophysical Research Letters*, 40(17), 4654–
790 4661. <https://doi.org/10.1002/grl.50896>
- 791 Godsey, S. E., Kirchner, J. W., & Tague, C. L. (2014). Effects of changes in winter snowpacks
792 on summer low flows: Case studies in the Sierra Nevada, California, USA. *Hydrological*
793 *Processes*, 28(19), 5048–5064. <https://doi.org/10.1002/hyp.9943>
- 794 Gorelick, N., Hancher, M., Dixon, M., Ilyushchenko, S., Thau, D., & Moore, R. (2017). Google
795 Earth Engine: Planetary-scale geospatial analysis for everyone. *Remote Sensing of*
796 *Environment*. <https://doi.org/10.1016/j.rse.2017.06.031>
- 797 Hale, K. E., Wlostowski, A. N., Badger, A. M., Musselman, K. N., Livneh, B., & Molotch, N. P.
798 (2022). Modeling streamflow sensitivity to climate warming and surface water inputs in a
799 montane catchment. *Journal of Hydrology: Regional Studies*, 39, 100976.
800 <https://doi.org/10.1016/j.ejrh.2021.100976>
- 801 Hall, D. K., & Riggs, G. A. (2007). Accuracy assessment of the MODIS snow products.
802 *Hydrological Processes*, 21(12), 1534–1547. <https://doi.org/10.1002/hyp.6715>

- 803 Hallema, D. W., Sun, G., Caldwell, P. V., Norman, S. P., Cohen, E. C., Liu, Y., Bladon, K. D., &
804 McNulty, S. G. (2018). Burned forests impact water supplies. *Nature Communications*,
805 9(1), 1307. <https://doi.org/10.1038/s41467-018-03735-6>
- 806 Hammond, J. C., Saavedra, F. A., & Kampf, S. K. (2018). How Does Snow Persistence Relate to
807 Annual Streamflow in Mountain Watersheds of the Western U.S. With Wet Maritime and
808 Dry Continental Climates? *Water Resources Research*, 54(4), 2605–2623.
809 <https://doi.org/10.1002/2017WR021899>
- 810 Harpold, A. A. (2016). Diverging sensitivity of soil water stress to changing snowmelt timing in
811 the Western U.S. *Advances in Water Resources*, 92, 116–129.
812 <https://doi.org/10.1016/j.advwatres.2016.03.017>
- 813 Hiemstra, C. A., Liston, G. E., & Reiners, W. A. (2006). Observing, modelling, and validating
814 snow redistribution by wind in a Wyoming upper treeline landscape. *Ecological*
815 *Modelling*, 197(1–2), 35–51. <https://doi.org/10.1016/j.ecolmodel.2006.03.005>
- 816 Jenicek, M., Seibert, J., & Staudinger, M. (2018). Modeling of Future Changes in Seasonal
817 Snowpack and Impacts on Summer Low Flows in Alpine Catchments. *Water Resources*
818 *Research*, 54(1), 538–556. <https://doi.org/10.1002/2017WR021648>
- 819 Li, D., Wrzesien, M. L., Durand, M., Adam, J., & Lettenmaier, D. P. (2017). How much runoff
820 originates as snow in the western United States, and how will that change in the future?
821 *Geophysical Research Letters*, 44(12), 6163–6172.
822 <https://doi.org/10.1002/2017GL073551>
- 823 Liston, G. E., & Elder, K. (2006a). A Meteorological Distribution System for High-Resolution
824 Terrestrial Modeling (MicroMet). *Journal of Hydrometeorology*, 7(2), 217–234.
825 <https://doi.org/10.1175/JHM486.1>

- 826 Liston, G. E., & Elder, K. (2006b). A Distributed Snow-Evolution Modeling System
827 (SnowModel). *Journal of Hydrometeorology*, 7(6), 1259–1276.
828 <https://doi.org/10.1175/JHM548.1>
- 829 Liston, G. E., Haehnel, R. B., Sturm, M., Hiemstra, C. A., Berezovskaya, S., & Tabler, R. D.
830 (2007). Simulating complex snow distributions in windy environments using SnowTran-
831 3D. *Journal of Glaciology*, 53(181), 241–256.
832 <https://doi.org/10.3189/172756507782202865>
- 833 Liston, G. E., & Hall, D. K. (1995). An energy-balance model of lake-ice evolution. *Journal of*
834 *Glaciology*, 41(138), 373–382. <https://doi.org/10.3189/S0022143000016245>
- 835 Liston, G. E., Hiemstra, C. A., Elder, K., & Cline, D. W. (2008). Mesocell Study Area Snow
836 Distributions for the Cold Land Processes Experiment (CLPX). *Journal of*
837 *Hydrometeorology*, 9(5), 957–976. <https://doi.org/10.1175/2008JHM869.1>
- 838 Luce, C. H., Abatzoglou, J. T., & Holden, Z. A. (2013). The Missing Mountain Water: Slower
839 Westerlies Decrease Orographic Enhancement in the Pacific Northwest USA. *Science*,
840 342(6164), 1360–1364. <https://doi.org/10.1126/science.1242335>
- 841 Lundquist, J. D., Dickerson-Lange, S. E., Lutz, J. A., & Cristea, N. C. (2013). Lower forest
842 density enhances snow retention in regions with warmer winters: A global framework
843 developed from plot-scale observations and modeling: Forests and Snow Retention.
844 *Water Resources Research*, 49(10), 6356–6370. <https://doi.org/10.1002/wrcr.20504>
- 845 Mauricio Zambrano-Bigiarini. (2020). *HydroGOF: Goodness-of-fit functions for comparison of*
846 *simulated and observed hydrological time series (0.4-0)*.
847 <https://doi.org/10.5281/zenodo.839854>

- 848 Moriasi, D. N., Arnold, J. G., Liew, M. W. V., Bingner, R. L., Harmel, R. D., & Veith, T. L.
849 (2007). Model Evaluation Guidelines for Systematic Quantification of Accuracy in
850 Watershed Simulations. *Transactions of the ASABE*, 50(3), 885–900.
851 <https://doi.org/10.13031/2013.23153>
- 852 Mote, P. W., Li, S., Lettenmaier, D. P., Xiao, M., & Engel, R. (2018). Dramatic declines in
853 snowpack in the western US. *Npj Climate and Atmospheric Science*, 1(1), 2.
854 <https://doi.org/10.1038/s41612-018-0012-1>
- 855 Musselman, K. N., Molotch, N. P., & Brooks, P. D. (2008). Effects of vegetation on snow
856 accumulation and ablation in a mid-latitude sub-alpine forest. *Hydrological Processes*,
857 22(15), 2767–2776. <https://doi.org/10.1002/hyp.7050>
- 858 NOAA, C. (2021). *Climate Data Online (CDO)-The National Climatic Data Center's (NCDC)*
859 *Climate Data Online (CDO) provides free access to NCDC's archive of historical*
860 *weather and climate data in addition to station history information.* | *National Climatic*
861 *Data Center (NCDC).*
- 862 R Core Team. (2021). *R: A Language and Environment for Statistical Computing*. R Foundation
863 for Statistical Computing. <https://www.R-project.org/>
- 864 Riggs, G. A., Hall, D. K., & Román, M. O. (2017). *Overview of NASA's MODIS and VIIRS*
865 *Snow-Cover Earth System Data Records* [Preprint]. Hydrology and Soil Science –
866 Hydrology. <https://doi.org/10.5194/essd-2017-25>
- 867 Saha, S., Moorthi, S., Wu, X., Wang, J., Nadiga, S., Tripp, P., Behringer, D., Hou, Y.-T.,
868 Chuang, H., Iredell, M., Ek, M., Meng, J., Yang, R., Mendez, M. P., Dool, H. van den,
869 Zhang, Q., Wang, W., Chen, M., & Becker, E. (2011). *NCEP Climate Forecast System*
870 *Version 2 (CFSv2) 6-hourly Products*. Research Data Archive at the National Center for

- 871 Atmospheric Research, Computational and Information Systems Laboratory.
872 <https://doi.org/10.5065/D61C1TXF>
- 873 Serreze, M. C., Clark, M. P., Armstrong, R. L., McGinnis, D. A., & Pulwarty, R. S. (1999).
874 Characteristics of the western United States snowpack from snowpack telemetry
875 (SNOTEL) data. *Water Resources Research*, 35(7), 2145–2160.
876 <https://doi.org/10.1029/1999WR900090>
- 877 Sexstone, G. A., Clow, D. W., Fassnacht, S. R., Liston, G. E., Hiemstra, C. A., Knowles, J. F., &
878 Penn, C. A. (2018). Snow Sublimation in Mountain Environments and Its Sensitivity to
879 Forest Disturbance and Climate Warming. *Water Resources Research*, 54(2), 1191–1211.
880 <https://doi.org/10.1002/2017WR021172>
- 881 Smoot, E. E., & Gleason, K. E. (2021). Forest Fires Reduce Snow-Water Storage and Advance
882 the Timing of Snowmelt across the Western U.S. *Water*, 13(24), Article 24.
883 <https://doi.org/10.3390/w13243533>
- 884 *SNOWpack TELEmetry Network (SNOTEL) | Ag Data Commons*. (2020).
885 <https://data.nal.usda.gov/dataset/snowpack-telemetry-network-snotel>
- 886 Stevens, J. T. (2017). Scale-dependent effects of post-fire canopy cover on snowpack depth in
887 montane coniferous forests. *Ecological Applications*, 27(6), 1888–1900.
888 <https://doi.org/10.1002/eap.1575>
- 889 Stevens-Rumann, C. S., & Morgan, P. (2019). Tree regeneration following wildfires in the
890 western US: A review. *Fire Ecology*, 15(1), 15. [https://doi.org/10.1186/s42408-019-](https://doi.org/10.1186/s42408-019-0032-1)
891 [0032-1](https://doi.org/10.1186/s42408-019-0032-1)
- 892 Ueyama, M., Ichii, K., Iwata, H., Euskirchen, E. S., Zona, D., Rocha, A. V., Harazono, Y.,
893 Iwama, C., Nakai, T., & Oechel, W. C. (2014). Change in surface energy balance in

894 Alaska due to fire and spring warming, based on upscaling eddy covariance
895 measurements: Change in high-latitude energy balance. *Journal of Geophysical*
896 *Research: Biogeosciences*, 119(10), 1947–1969. <https://doi.org/10.1002/2014JG002717>

897 U.S. Geological Survey National Geospatial Program. (2022). *USGS National Hydrography*
898 *Dataset Plus High Resolution National Release 1 FileGDB* [Data set]. U.S. Geological
899 Survey. <https://doi.org/10.5066/P9WFOBQI>

900 *USGS Water Data for the Nation*. (2022). <https://waterdata.usgs.gov/nwis>

901 Varhola, A., Coops, N. C., Weiler, M., & Moore, R. D. (2010). Forest canopy effects on snow
902 accumulation and ablation: An integrative review of empirical results. *Journal of*
903 *Hydrology*, 392(3–4), 219–233. <https://doi.org/10.1016/j.jhydrol.2010.08.009>

904 Venables, W. N., & Ripley, B. D. (2002). *Modern Applied Statistics with S* (Fourth). Springer.
905 <https://www.stats.ox.ac.uk/pub/MASS4/>

906 Westerling, A. L. (2016). Increasing western US forest wildfire activity: Sensitivity to changes in
907 the timing of spring. *Philosophical Transactions of the Royal Society B: Biological*
908 *Sciences*, 371(1696), 20150178. <https://doi.org/10.1098/rstb.2015.0178>

909 Western Regional Climate Center. (2021). *RAWS USA Climate Archive*. <https://raws.dri.edu/>

910 Wieder, W. R., Kennedy, D., Lehner, F., Musselman, K. N., Rodgers, K. B., Rosenbloom, N.,
911 Simpson, I. R., & Yamaguchi, R. (2022). Pervasive alterations to snow-dominated
912 ecosystem functions under climate change. *Proceedings of the National Academy of*
913 *Sciences*, 119(30), e2202393119. <https://doi.org/10.1073/pnas.2202393119>

914 Yuan, X., Wood, E. F., Luo, L., & Pan, M. (2011). A first look at Climate Forecast System
915 version 2 (CFSv2) for hydrological seasonal prediction: A FIRST LOOK AT CFSv2.
916 *Geophysical Research Letters*, 38(13), n/a-n/a. <https://doi.org/10.1029/2011GL047792>

917

918 **Appendix A: Snowpack Energy Balance and Significance Testing**

919 Supporting plots and tables for postfire snowpack energy balance and supporting significance
 920 values for figures and tables included in the body of the text.

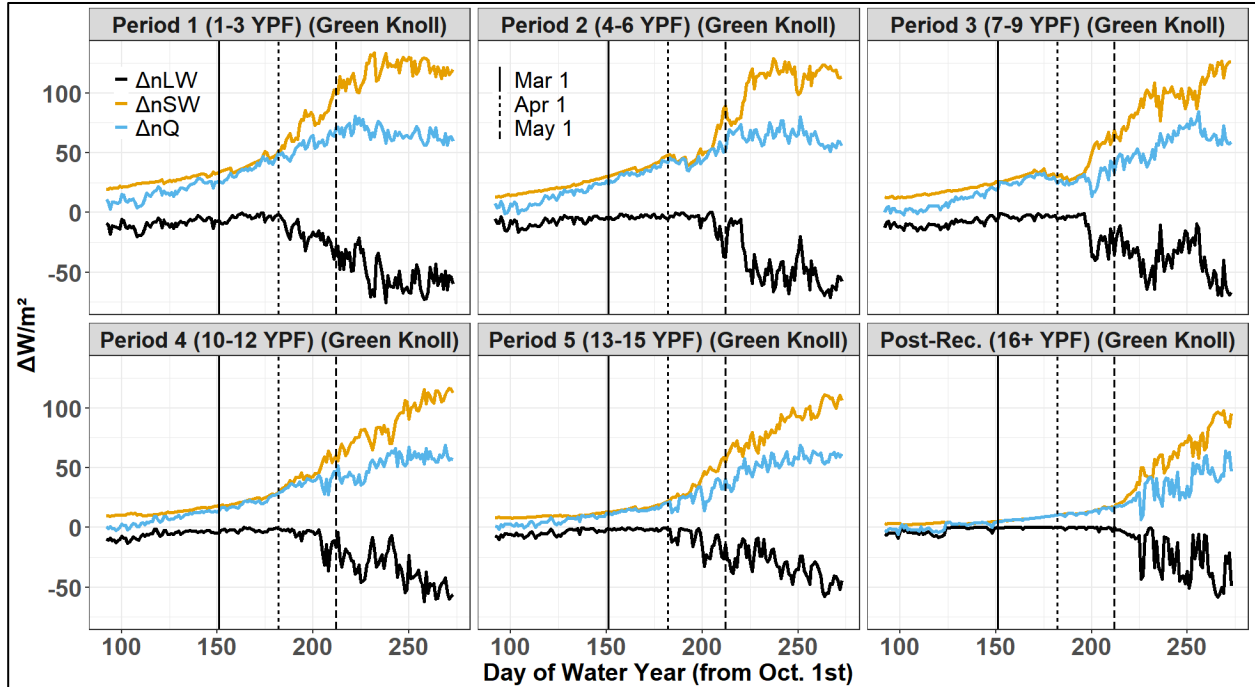


Figure A1: Difference between base model and postfire albedo model net components of the snowpack energy balance averaged over 3-year bins since burn for the Green Knoll forest fire only.

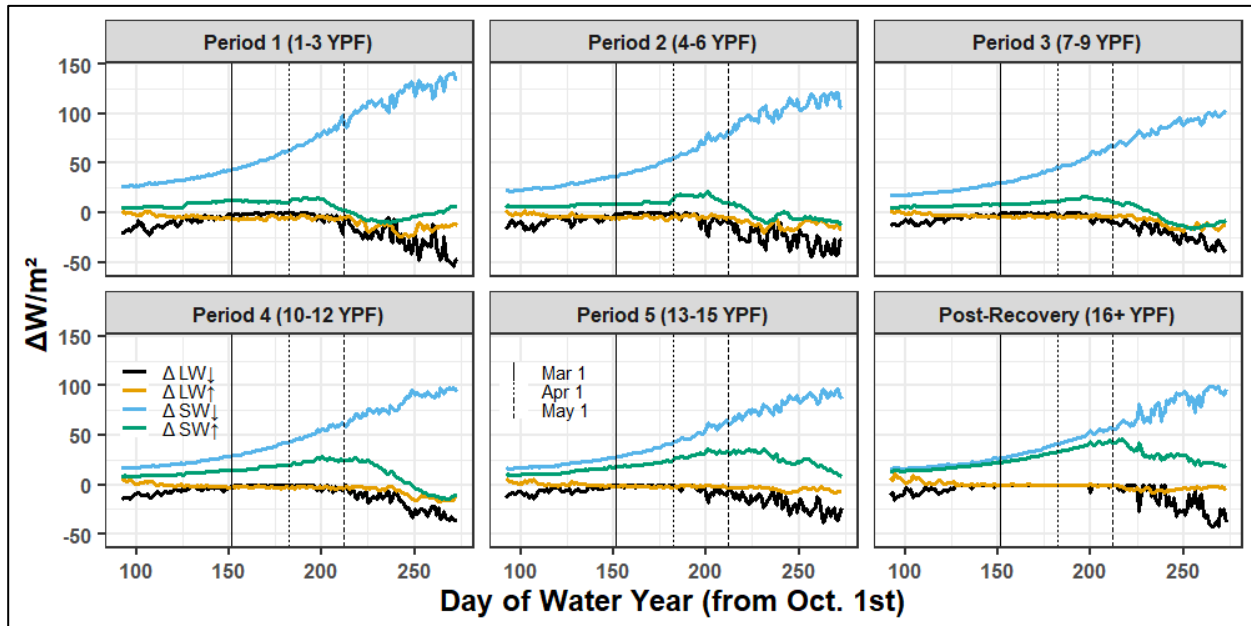


Figure A2: Difference between base model and postfire albedo model net components of the snowpack energy balance averaged over 3-year bins since burn over all modeled forest fires.

Table A1: Numerical results of significance testing performed on all modeled SWE results. For each result, 100 random pixels between the base model and postfire albedo model were selected and a two-sided Welch Two-Sample t-test was performed with an alpha value of 0.05.

Immediate Losses p-values Welch Two-Sample t-test; two-sided; $\alpha = 0.05$; $n = 100$								
	Boulder	Green Knoll	Purdy	Bull	Horsethief Canyon	Lava Mountain	Cliff Creek	Roosevelt
p-value	1.58E-04	0.0479	0.0016	0.438	1.12E-05	3.21E-18	1.99E-06	0.00261
Total Losses p-values Welch Two-Sample t-test; two-sided; $\alpha = 0.05$; $n = 100$								
	Boulder	Green Knoll	Purdy	Bull	Horsethief Canyon	Lava Mountain	Cliff Creek	Roosevelt
p-value	0.086	4.42E-04	0.420	0.0134	0.0045	1.71E-03	0.0041	0.0062
Period Averaged Peak SWE p-values Welch Two-Sample t-test; two-sided; $\alpha = 0.05$; $n = 100$								
	Boulder	Green Knoll	Purdy	Bull	Horsethief Canyon	Lava Mountain	Cliff Creek	Roosevelt
Period 1	1.35E-33	1.39E-33	0.00270	3.71E-04	6.22E-15	0.450	0.811	0.00559
Period 2	3.59E-07	8.04E-17	0.00436	5.23E-18	0.00367	0.00498	4.30E-05	
Period 3	0.00960	0.0023	3.22E-06	0.207	0.245			
Period 4	1.58E-22	0.0744	1.26E-14	0.834				
Period 5	0.414	0.00408	2.17E-08					
Post-Rec.	1.35E-08	4.74E-27						
March 1st SWE p-values Welch Two-Sample t-test; two-sided; $\alpha = 0.05$; $n = 100$								
	Boulder	Green Knoll	Purdy	Bull	Horsethief Canyon	Lava Mountain	Cliff Creek	Roosevelt
Period 1	4.84E-59	2.45E-34	2.82E-21	1.08E-25	1.23E-31	0.156	0.247	0.0176
Period 2	0.501	2.69E-24	1.29E-44	1.77E-18	1.66E-13	7.21E-47	1.61E-24	
Period 3	0.0406	4.80E-06	2.23E-27	0.213	9.84E-07			
Period 4	0.381	2.86E-13	0.0494	2.96E-25				
Period 5	0.00444	1.19E-05	6.21E-61					
Post-Rec.	4.94E-52	9.17E-44						
April 1st SWE p-values Welch Two-Sample t-test; two-sided; $\alpha = 0.05$; $n = 100$								
	Boulder	Green Knoll	Purdy	Bull	Horsethief Canyon	Lava Mountain	Cliff Creek	Roosevelt
Period 1	0.00152	2.77E-29	7.66E-09	2.90E-06	2.34E-17	3.20E-07	0.00245	0.144
Period 2	0.813	1.64E-20	0.00812	0.0328	0.0600	0.0159	0.0224	
Period 3	0.00679	0.574	0.101	2.36E-05	0.290			
Period 4	7.48E-19	9.67E-11	3.39E-23	0.0336				
Period 5	1.26E-05	0.109	3.01E-12					
Post-Rec.	1.13E-16	2.72E-08						
May 1st SWE p-values Welch Two-Sample t-test; two-sided; $\alpha = 0.05$; $n = 100$								
	Boulder	Green Knoll	Purdy	Bull	Horsethief Canyon	Lava Mountain	Cliff Creek	Roosevelt
Period 1	4.52E-101	4.07E-61	0.546	3.80E-05	5.39E-22	0.383	1.17E-07	4.27E-11
Period 2	1.63E-56	3.11E-30	0.0279	3.32E-27	2.42E-06	2.35E-12	3.01E-14	
Period 3	1.20E-19	0.232	0.199	0.0157	6.48E-08			
Period 4	1.09E-08	2.22E-04	5.82E-23	0.846				
Period 5	0.204	9.76E-18	0.00342					
Post-Rec.	1.58E-26	2.93E-06						

924 Table A2: Net shortwave radiative forcing (netSW) on snowpack averaged across all forest fires for the base model,
 925 the postfire forest recovery model (Forest) and postfire snow albedo recovery model (Albedo) and the change in
 netSW attributable to postfire degradation of forest structure ($\Delta nSW_{\text{forest}}$) or postfire effects on snow albedo
 ($\Delta nSW_{\text{albedo}}$).

		Accumulation (net SW)			Attribution (absolute)		Attribution (proportional)	
		Base Model	Forest Model	Albedo Model	$\Delta nSW_{\text{forest}}$	$\Delta nSW_{\text{albedo}}$	$\Delta nSW_{\text{forest}}$	$\Delta nSW_{\text{albedo}}$
Period		Mean (W/m ²)	Mean (W/m ²)	Mean (W/m ²)	(W/m ²)	(W/m ²)	(%)	(%)
1		20.6 ± 2.76	43.2 ± 6.06	61.0 ± 9.16	22.6	17.8	52.3	29.2
2		24.1 ± 2.77	43.7 ± 5.49	59.1 ± 7.45	19.6	15.4	44.9	26.1
3		26.2 ± 2.79	41.5 ± 4.76	52.9 ± 6.17	15.3	11.4	36.9	21.6
4		23.8 ± 2.74	35.2 ± 4.31	41.8 ± 5.20	11.4	6.60	32.4	15.8
5		26.2 ± 3.53	35.8 ± 5.14	39.6 ± 5.87	9.60	3.80	26.8	9.60
Post-rec.		24.1 ± 2.79	29.7 ± 3.74	29.7 ± 3.74	5.60	0.00	18.9	0.00
		Ablation (net SW)			Attribution (absolute)		Attribution (proportional)	
		Base Model	Forest Model	Albedo Model	$\Delta nSW_{\text{forest}}$	$\Delta nSW_{\text{albedo}}$	$\Delta nSW_{\text{forest}}$	$\Delta nSW_{\text{albedo}}$
Period		Mean (W/m ²)	Mean (W/m ²)	Mean (W/m ²)	(W/m ²)	(W/m ²)	(%)	(%)
1		31.6 ± 5.05	68.7 ± 12.5	96.3 ± 17.3	37.1	27.6	54.0	28.7
2		33.4 ± 5.11	63.7 ± 10.6	85.1 ± 14.9	30.3	21.4	47.6	25.1
3		37.5 ± 4.80	61.3 ± 8.79	78.9 ± 11.7	23.8	17.6	38.8	22.3
4		34.1 ± 4.20	53.1 ± 7.33	62.6 ± 8.48	19.0	9.50	35.8	15.2
5		38.4 ± 5.92	54.6 ± 9.35	60.3 ± 10.3	16.2	5.70	29.7	9.45
Post-rec.		37.8 ± 5.11	48.0 ± 6.86	48.1 ± 6.92	10.2	0.10	21.3	0.21

Table A3: Net longwave radiative forcing on snowpack across all forest fires for both the base model (Base) and
 postfire snow albedo recovery model (Forest + Albedo) and the difference between the two models (Diff).

		Accumulation (net LW)					Ablation (net LW)				
		Base Model		Forest + Albedo Model			Base Model		Forest + Albedo Model		
Period		Mean (W/m ²)	SD (W/m ²)	Mean (W/m ²)	SD (W/m ²)	Diff (F&A - B) (W/m ²)	Mean (W/m ²)	SD (W/m ²)	Mean (W/m ²)	SD (W/m ²)	Diff (F&A - B) (W/m ²)
1		581	19.4	587.0	18.5	6.00	603	11.8	608	11.5	5.00
2		586	12	591	11.1	5.00	595	15.9	599	15	4.00
3		577	16.2	581	15.7	4.00	592	12.4	596	12	4.00
4		582	17.7	584	17.50	2.00	601	13.5	604	13.2	3.00
5		578	17.8	579	18.2	1.00	598	17.2	600	17.3	2.00
Post-rec.		606.0	15.4	606	15.3	0.00	624	12.1	624	12	0.00